Politecnico di Torino

Massachusetts Institute of Technology

Effects of helium-ion exposure on superconducting nanowires single photon detectors

Master's Degree Programme NanoQuad

Francesca Incalza

Université Paris Cité and Politecnico di Torino
Quantum Nanostructures and Nanofabrication group at
Massachusetts Institute of Technology (MIT), Cambridge

Supervision

Prof. Carlo Ricciardi
Prof. Karl K. Berggren

July 1, 2023

Twenty years from now, you will be more disappointed by the things you didn't do than by the ones you did do. So throw off the bowlines. Sail away from the safe harbor. Catch the trade winds in your sails. Explore. Dream. Discover.

-Mark Twain

A mia madre, mio padre, Antonio e Andrea

Abstract

Ultra-fast single-photon detectors can be useful for a lot of different applications, including quantum optical communication systems, high-speed communication, lightweight cryogenics for space crafts and biomedical use. In particular, high-temperature superconductors can allow for the development of superconducting nanowire single photon detectors (SNSPDs) that can operate at higher temperatures than standard superconductors, enhancing efficiency, simplicity of use, viability and affordability of the device in quantum computing, communications, and sensing. Despite this, it has to be pointed out that so far the fabrication of high temperature superconducting nanowires struggles to preserve good properties. Moreover, current state of the art sees the need for large and uniform detectors arrays formed by hundreds or thousands of detectors. As a results, the opportunity of modification of the detector metrics through post-processing gained more and more attention. In this thesis we try to investigate the effects of ion irradiation on superconductive nanowires single photon detectors. MgB_2 and NbN have been chosen for our detectors and helium as irradiating ion. We were able to demonstrate the impact of different doses on the target materials as well as the ability of improving the detector metrics that could lead to the possibility of reaching homogeneous detector metrics after fabrication and on the same chip.

Acknowledgements

I would like to express my heartfelt gratitude to all the wonderful people who have been by my side throughout this amazing journey. Their support, encouragement, and contributions have been fundamental for me.
I thank Prof. Karl Berggren for believing in me and providing me with the incredible and invaluable opportunity to work alongside him and his team.
I thank Prof. Maria Luisa Della Rocca and Prof. Carlo Ricciardi for their participation on my thesis committee and their unwavering support and guidance.
I thank Matteo Castellani and Emma Batson for fabricating my devices, dedicating their time overnight to assist me with the measurements, and for being exceptional colleagues and a constant source of inspiration. I am truly grateful for everything.
I thank Dip Joti Paul, Owen Medeiros, Marco Colangelo and all the members of the QNN group. I am immensely thankful for your help, assistance and advises. They have been precious and indispensable for me.
I thank Sandro Buzzi for his help with images and his pleasant company and support.
I thank Jim Daley for his patient guidance and commitment during the training process.
I thank Dorothy Fleischer and Rinske Wijtmans Robinson for your kind assistance in handling all my administrative issues.
I thank my roommates Marco Raffa and Marco Zagarella for being by my side in the good and tough moments of this journey. Your presence has been vital for me over the past months.
I thank all my friends, near and far, in my hometown, in Turin, Paris and Boston. Your love has enriched my days in immeasurable ways.
I thank my grandmother and my grandfather for their immense love and support. Your wisdom, kindness, and enduring presence has fueled my determination to overcome challenges and pursue my dreams.
I thank my parents Letizia and Giuseppe, and my brothers Antonio and Andrea. You are the foundation of everything I am and aspire to be. You teach me how to follow my dream and to believe in myself. Thank you for your advising, listening, warning, supporting, criticizing, teaching, inspiring and reminding me of what truly matters in life.

Contents

Chapter 1

Introduction

This chapter initially explains the fundamentals of superconducting nanowire single-photon detectors, such as the detection mechanism, the principal parameter and future objectives. The motivation and purpose of this thesis is then described.

1.1 Superconducting nanowire single photon detectors

Superconducting nanowire single photon detectors (SNSPDs) have made significant strides over the past two decades, from initial proofs of concept to integrated circuits and a wide range of applications, including high-speed communication, quantum information, quantum key distribution, biomedical imaging, light detection and ranging (LIDAR), and deep space communication [1]. SNSPDs are based on the transition from the superconducting to the normal state in a superconducting nanowire. One incoming photon can split apart hundreds of Cooper pairs, creating a hotspot (an area of material in the normal state) [2]. As the normal zone expands, a transient resistance state is created, which causes a voltage pulse to appear in the read-out circuit and signify a detection event. The nanowire returns to the superconducting state after some relaxation time set by properties of the system like heat transfer, kinetic inductance and shunt resistance.

The degree of performance of these SNSPDs is determined by properties of the microstrips or nanowires that are the essential components of such devices, and they are often made from superconducting ultrathin films using micro-nanofabrication techniques. However, despite the high efficiencies found up to this moment, these devices need the usage of liquid helium or multi-stage cryocoolers which puts restrictions on the practical device applications. High-temperature superconductors are suitable materials for SNSPDs to have better accessibility and convenience. The crucial point is to rise above liquid helium temperatures in order to avoid the need for cryostats, giving advantages in terms of scalability and costs. For example, niobium nitride is a type II superconductor that exhibits a critical temperature of 8-9 K in the thin film configuration. In this case, operations are limited to temperatures at least lower than $\frac{1}{2}\ T_c$ (sub-4K), easily obtainable with liquid helium (4.2 K). Another interesting material, magnesium diboride (MgB_2), is currently under study because it seems to possess very useful properties for the aforementioned goals. Magnesium diboride can be considered a two-gap high-temperature conventional superconductor, which indicates an electron-phonon mechanism of superconductivity that can be described within the BCS (Bardeen-Cooper-Schrieffer) scenario. A search for high-temperature conventional superconductivity is likely to be fruitful, as the Bardeen–Cooper–Schrieffer (BCS) theory in the Eliashberg formulation puts no apparent limits on Tc. Materials with light elements are especially favorable as they provide high frequencies in the phonon spectrum, strong electron-phonon

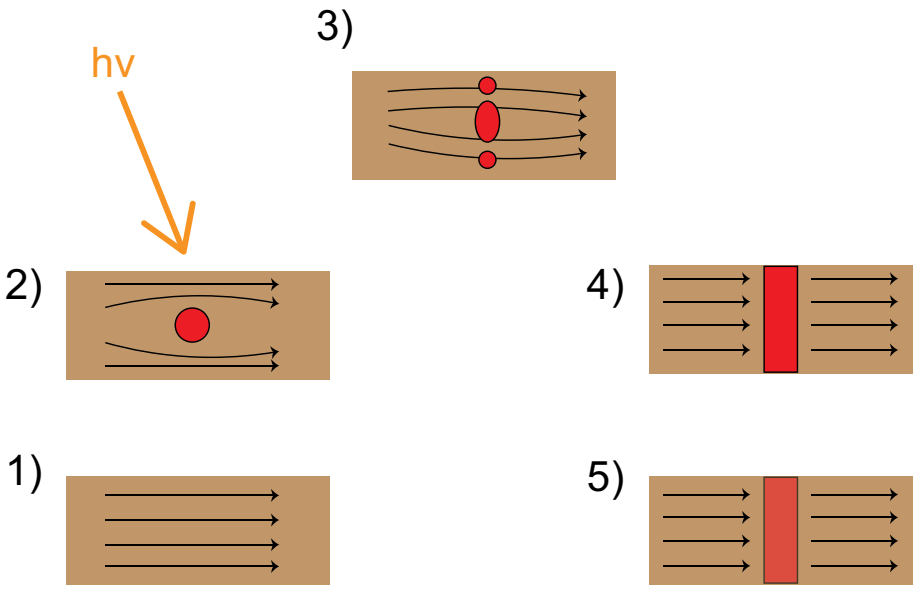

Figure 1.1: Schematic of the normal-core hotspot model. The detection is divided into 5 steps: 1) The superconducting nanowire is below the critical temperature (black arrows are the bias current). 2) The resistive hotspot is created due to the incident photon. 3) Diffiusion of the hotspot. 4) A voltage pulse can now be read. (5) The resistive barrier vanishes, diffusing into the substrate. The cycle can restart.

coupling, and a high density of states. This is, indeed, the case of the moderately high T_c (39 K for the bulk) MgB_2 [3]. Despite this, it has to be pointed out that thin film superconducting nanowires struggles to preserve the same high critical temperature (T_c) and desired properties of the bulk. Indeed, good material quality is hard to achieve when dealing with thin films, particularly in terms of defects and uniformity determined at the early stages of growth as well as of fabrication process of nanowires that tends to damage fragile high-T_c superconductors. Indeed, high-T_c superconductors are often chemically tough oxides that can not be etched. For this reason, ion milling is usually used, i.e, mechanically removing the material, causing a lot of heating and damage. Even if current state-of-the-art SNSPDs combine near-unity detection efficiency over a wide spectral range, low dark counts, short dead times, and picosecond time resolution, more and more attention is going towards the requirement for high temperatures of operation as well as large detector arrays and good homogeneity within an ensemble of thousands of detectors [1]. For this reason, post-processing tools are gaining attention with the aim of tuning the detector metrics of individual devices fabricated on the same chip.

1.2 Towards high-T_c SNSPDs using ion exposure

The effects of helium-ion exposures on superconducting thin films have drawn a lot of interest because of the possible performance attained in fields like single-photon detection and electronics [4]. In particular, helium ion exposure can be used to address the problems we mentioned before: with larger doses, it can be used to directly pattern films; at low levels, it may modify materials leading to different properties which can enhance device performance. A beam of helium ions is focused on the material, accelerated to particular velocities and energies. The process is performed at low temperatures, allows for an instant-on/off control and a precise control of implanting current and charge that allow for better control of the implanted dose that can be monitored in situ. Increased implant energies can

allow for the penetration into thin films of materials, with the peak of implanted dopant profiles below the surface (buried). The ion energy and the dose are important control parameters: the first, for the depth of the implant and the amount of crystal damage created; the second, for the control of the concentration. Different effects on the target material are expected when different irradiation doses are applied. For this reason, data from the dose test is important to inform the nanowire fabrication process, that is the estimation of the dose at which the thin film is modified and, eventually, the superconductivity suppressed [5].

Indeed, as said before, the impact of He ions on the properties of superconductors can be exploited to obtain advantages in terms of fabrication and efficiency of the device. By controlling the irradiation dose, for instance, "direct-written" tunnel barriers could be created undergoing a transition from superconductor to an insulator as irradiation dose is increased [6] as well as Josephson nano-junctions with the lowest noise level possible [7]. For instance, more specifically, to produce well-defined MgB_2 nanowires from ultrathin films while maintaining the high T_c focused ion beam (FIB) milling is used by accurately etching directly tiny details into a material, controlling the strength and direction of the ions, with no need of prior patterning processes. For example, Zhang et al. were able to fabricate high quality superconducting nanowires from HPCVD-prepared MgB_2 films in 10 nm thick by using a FIB milling technique [8]. High-Pressure Chemical Vapor Deposition (HPCVD) allows to obtain a starting superconducting film with good adhesion, uniformity and precise control over composition, thickness, and crystallinity. Zhang et al. obtained MgB_2 nanowires in widths of 320-650 nm with a T_c above 34 K and superconducting critical current density above $5 \cdot 10^7$ A/cm^2 at 20 K, demonstrating potential in making MgB_2-based nano-devices with high operating temperatures [8]. Moreover, in order to shield the MgB_2 nanowires from contamination during the FIB process, protective layers of Ti/Au can be deposited onto the ultrathin films. In fact, impurities and defects around the wire edges of superconducting devices can result in local current crowding and so decrease performance.

Using He^+ ion irradiation to directly patter devices would reduce the number of steps needed in the fabrication process and potentially lessen the probability of damaging the material, allowing to improve the quality of the superconducting nanowires [5]. Moreover, it has been shown that an increase of the intrinsic detection efficiency (IDE) can be obtained thanks to the irradiation-induced reduction of the superconducting energy gap and the electron density of states at the Fermi level [2]. In fact, it seems that after the photon absorption, the normal state is more easily obtained probably because of the ion-induced atom dislocation mechanism that causes interband scattering. Intrinsic detection efficiency (IDE) is the probability of a pulse generation in the nanowire when a photon is absorbed. In realizing a SNSPD with system detection efficiency (SDE) near unity, all the factors that affect the SDE (i.e., IDE, AE, and OCE) must be optimized simultaneously, where AE is the optical absorption efficiency and OCE is the optical coupling efficiency. Through helium-ion exposures a saturation of the IDE is obtained keeping the SDE high and without changing a lot the AE in the telecommunication range (1550 nm) and without modifying the geometry. As said before, it seems that the dose test could be very important also in this case. Indeed, W. Zhang et al. showed the decrease of the T_c with the increase of created vacancies by helium irradiation into NbN as well as the increase of the broadening of δT_c in a magnetic field being evidence of an increasing lattice disorder. Regarding this, further theoretical study is required to understand and predict this. Moreover, an exposure of He^+ ions on MgB_2 with negligible effects on the T_c, I_{sw} and normal state resistance was experimentally demonstrated, establishing a new route for the development of high-T_c quantum sensors and their use in space communication [9]. Correlated to the aforementioned case, experimental evidence of MgB_2

microwires with sub-ns response with a high count rate of up to 100 MHz at 20 K has been demonstrated [10]. Likely, in order to understand how to exploit the helium irradiation on superconductive thin films, it would be also important to study the irradiation damage on the considered material. X-ray diffraction (XRD) and X-ray reflectometry (XRR) could be a potential tool to investigate how the local environment around atoms is influenced by point defects induced by $He+$ ion irradiation [11].

1.3 This thesis

The purpose of this thesis is to use local He^+ ion irradiation to modify the electrical and optical properties of superconductive thin films. Specifically, we conducted irradiation experiments on SNSPDs (Superconducting Nanowire Single-Photon Detectors), as well as nanowires of MgB_2 and NbN. Our investigation focused on understanding the impact of ion irradiation on the material properties, particularly in terms of superconducting behavior, detector performance metrics, and the feasibility of fabricating passive functional elements (such as resistors and capacitors) by adjusting the radiation dosage.

1.4 Quantum Nanostructure and Nanofabrication Group

Quantum Nanostructure and Nanofabrication Group (QNN) is a dynamic and innovative team dedicated to advancing the field of electronic and photonic devices through nanoscience and nanotechnology research. The group belongs to the Department of Electrical Engineering and Computer Science (EECS) of Massachusetts Institute of Technology and Professor Karl K. Berggren is the principal investigator.

With a focus on advance nanofabrication technology to the few-nanometer length scale, the group aims to explore new technologies to push the boundaries of current-state of the art of photonic and electrical devices, by combining electrical engineering, physics, and materials science. The group brings together a diverse range of experts, including materials-scientists, physicists, chemists, and electrical engineers. Through collaborative efforts and a multidisciplinary approach, the Group is working on creating the best light detecting technologies, which have high sensitivity, a wide spectral range, a quick reset time, and high timing precision, With a special emphasis on the nanowire-based superconductive photodetectors. In particular, for a wide range of applications, including communication, quantum computation, microscopy and spectroscopy, as well as optical and thermal imaging systems, it is crucial to resolve the information concealed in a light signal. Superconducting nanowire-based single photon detectors (SNSPDs) are an essential technology which is modeled, constructed, analyzed, and used in the group. The combination of advanced nanofabrication techniques with nano-optics and thermoelectric theories, as well as by using low-temperature, very quick, and highly sensitive optical and electrical characterization techniques and instruments is the main focus of QNN group.

Chapter 2

Stopping and Range of Ions in Matter (SRIM) Simulation

In this chapter we analyze the properties of He ion irradiation in high-temperature superconductors, such as MgB_2 and NbN, and the consequences that the different parameters may have on it. To do this, we used a Monte Carlo simulation software package called SRIM (Stopping and Range of Ions in Matter). This tool is used to simulate the behavior of ions in matter in the field of ion implantation and ion beam analysis, as well as in the study of radiation damage in materials.

2.1 Ion distribution

The final distribution of the ions irradiated into a target material which refers to the spatial arrangement and characteristics of the ion implantation process will allow the analysis of the irradiation process. In figure 2.1, the abscissa shows the depth of the ions penetrating into the target and the ordinate, in units of $\frac{Atoms/\mathrm{cm}^3}{Atoms/\mathrm{cm}^2}$, is representing a value that multiplied by an ion-beam dose (normally in units of $Atoms/\mathrm{cm}^2$) gives directly a concentration of ions per cm^3. In particular, this ion distribution plot can provide us information about the characteristics of the ion implantation process, such as the implantation depth, the ion range, and the peak concentration of implanted ions. Moreover, this plot can be used to identify any anomalies or non-uniformities in the ion distribution that may be caused by scattering or other physical processes, helping the understanding of the behavior of ions in the material and optimizing the design of ion implantation processes itself.
We started with the simulation over a bare MgB_2 film and in figure 2.1, we can observe the interaction of 20 keV helium ion with a bulk MgB_2 film of 1000 Å. In particular, the ion range is defined as the total distance the ion travels in coming to rest and the straggle is the statistical fluctuation along an axis perpendicular to the axis of incidence or the standard deviation in plane perpendicular to the surface. It can be defined as the distance an ion travels in a material before stopping or losing a substantial amount of energy due to interactions with atoms or electrons. The ion range is an important parameter in ion implantation processes, as it determines the depth at which ions are implanted into a material, as well as in ion beam analysis techniques, where the range of ions is used to investigate the composition and structure of materials by measuring the energy loss of ions as they penetrate the material. The ion range of 690 Å obtained for the bulk MgB_2 target will be used as a reference for comparison with the thin film case we are interested in for our applications.
The simulated structure has been chosen coherently with the real device under test, that is a thin

layer of MgB_2 between two protective layers of MgO onto a SiC substrate which results to be the best material for a good lattice match and a thin layer of NbN onto a SiO_2/Si substrate (figure 2.2 and 2.3). The first important parameter that has been considered is the thickness of the superconducting layer. Indeed, to obtain an ultra-fast superconducting nanowire single-photon detectors, the amount of time

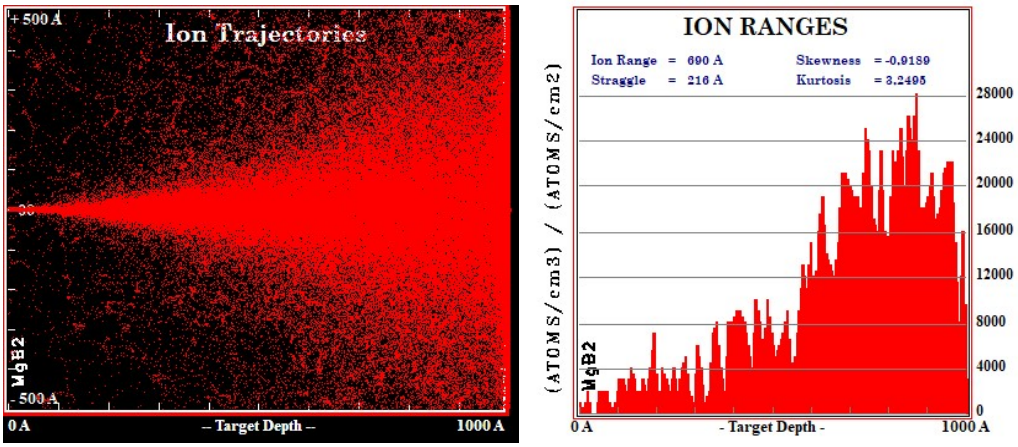

(a) **(b)**

Figure 2.1: Simulation of the interaction of Helium ions with an acceleration voltage of 20 keV on a bulk MgB_2 target.

needed to resume the superconducting state after the detection of a photon, know as reset time, needs to be reduced as much as possible.
This reset time, τ is directly proportional to the kinetic inductance, L_k, through the load resistance R_{load}:

$$\tau = \frac{L_k}{R_{load}} \tag{2.1}$$

Moreover, in order to prevent latching into a resistive state, non-equilibrium quasiparticles must recombine very fast into Cooper pairs and so a fast thermal relaxation time, set by electron-phonon and electron-electron interactions, is needed [12].
So, superconducting nanowires with both low kinetic inductance and fast electron energy relaxation are required to lower the reset time.
The kinetic inductance is related to the mass of the charge carriers in the superconducting material, so that lighter carriers lead to lower kinetic inductance. The latter can be indeed defined, following the Drude model, as:

$$L_k = \frac{m^*}{n_s q^2}, \tag{2.2}$$

where m^* is the effective mass, n_s the the charge carrier density and q the elementary charge. Moreover, by defining λ_{eff} as the effective magnetic penetration depth of a dirty bulk superconductor, given by

$$\lambda_{eff} = \lambda_L \sqrt{\frac{\xi_0}{l}} \tag{2.3}$$

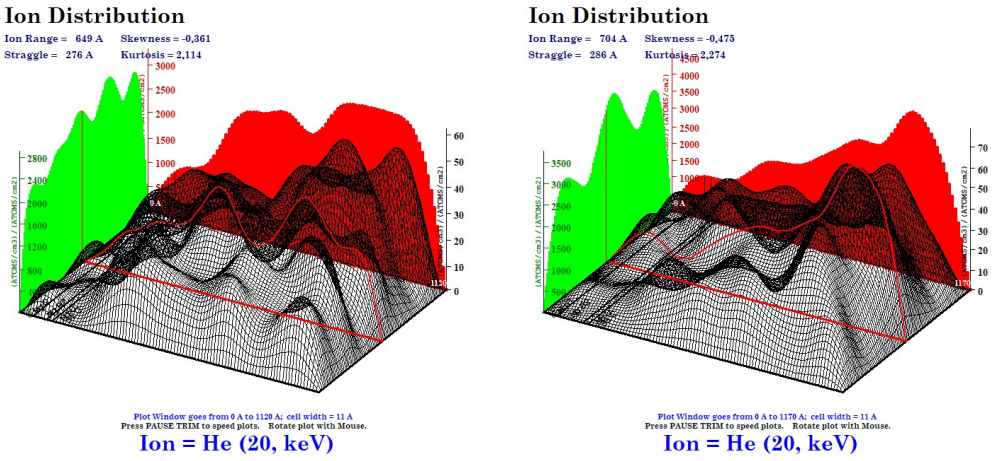

(a) **(b)**

Figure 2.2: Simulation of the interaction of Helium ions with an acceleration voltage of 20 keV at 5 and 10 nm thick MgB_2 target, with resulting ion range of 649 and 704 Å respectively. A slightly higher ion concentration peak is observed in the 10 nm film.

where λ_L is the London penetration depth, ξ_0 the BCS coherence length and l the mean free path, the kinetic inductance, in the case of a thin film ($d \ll \lambda_{eff}$), depends on the thickness through

$$L_k = \frac{\mu_0 \lambda_{eff}^2 l}{dw} = \frac{\hbar R_{sheet} l}{\pi \Delta(0\ \mathrm{K}) w} \tag{2.4}$$

with l, w, and d are respectively length, width and thickness and where ρ the specific resistivity of the superconducting film in the normal conducting state, and $\Delta(0\ \mathrm{K})$ the superconducting energy gap [13, 14, 15]. From this formula, we can deduce that in order to decrease L_k, and so the reset time, the thickness of the film and the dose of the irradiation are effective parameters through the sheet resistance. It's feasible that the understanding of the differences in terms of electron relaxation time, and so of different scattering events, and He penetration into different film thicknesses will be useful to find the good configuration for ultra-fast SNSPDs. From the simulation of different thicknesses it turns out that the bigger differences in terms of ion distributions can be found only between the ranges of 5 and 10 nm thick films for MgB_2 and slightly higher for NbN, i.e more or less between 8 and 20 nm. Actually, even if the difference appears to be negligible, it's possible that the little higher concentration of He ions in the superconductive film will change the electron relaxation time due to different scattering events. Moreover, this simulation tool allows to estimate characteristic doses needed to introduce a significant amount of defects and damages into the target material (in our case MgB_2 crystal lattice or polycristalline NbN) even, eventually, up to the suppression of superconductivity [9]. More specifically, with reference to the MgB_2 in order to obtain an ion damage of around $5 * 10^{19}$ ion/cm^3, a dose of at $5 \cdot 10^{15}$ ions/cm^2 is needed and a damage of more or less 10^{18} ions/cm^3 with doses of He ions around 10^{14} ions/cm^2. Experimentally, we're going to try to determine which dose could be effective to get the right amount of damage, for instance characterizing the samples using transport measurements in order to identify those with pronounced hysteresis in the I-V curves (see chapter 4).

In the case of niobium nitride thin films, the ion range results to be higher with respect to the MgB_2 (see 2.3). As a result, it is plausible that lower exposure doses are need on this material to obtain the modification of the superconducting properties and for the destruction of the superconductivity itself

Helium and Xenon irradiation on 5 nm MgB_2 (20 keV)			
	MgB_2 with Si capping layer (He)	MgB_2 without Si capping layer (He)	MgB_2 without Si capping layer (Xe)
Ion range (Å)	772	756	124
Total vacancies	39/ion	38/ion	220/ion
Straggle (Å)	252	253	28
Skewness	-0.836	-0.835	0.212

Table 2.1: Parameters of He and Xe ion exposure on different MgB_2 stacking configurations.

Irradiation of NbN/SiO/Si (15 nm, 300 nm, 100nm)			
	He	Ar	Ga
Ion range (Å)	1543	123	84
Total vacancies	61/ion	199/ion	225/ion
Straggle (Å)	565	72	45
Skewness	-0.348	0.879	0.899

Table 2.2: Parameters of different ion exposure on NbN/SiO/Si.

through irradiation. Indeed, in this case a dose of 10^{14} ions/cm^2 would generate a damage of around 10^{19} ions/cm^3. This results is pretty relevant on the experimental point of view. Moreover, thanks

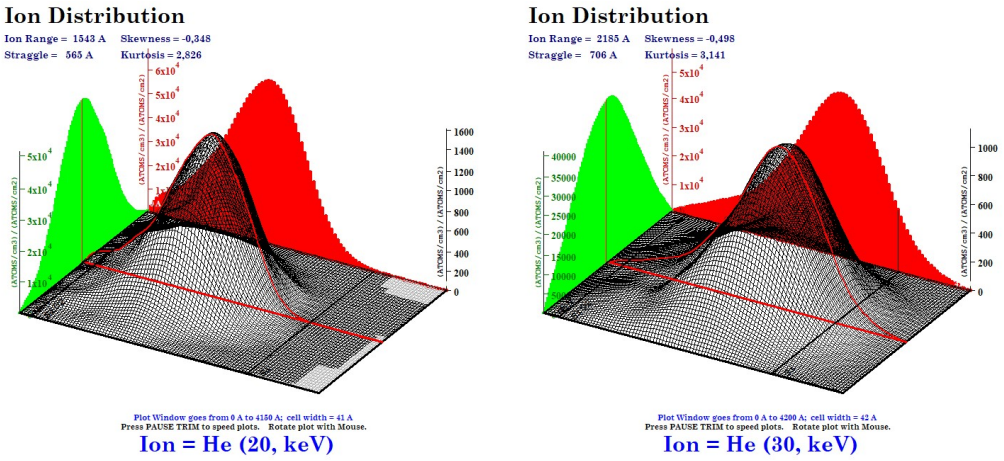

(a) **(b)**

Figure 2.3: Interaction of He ions with the NbN 15 nm and 20 nm thin film (2.3a and 2.3b respectively). Higher ion ranges with respect to the MgB_2 can be observed (2000 Å).

to the SRIM simulation tool, we were able to compare different parameters with an important rule in ion irradiation. Particularly, we simulated the ion range, the total vacancies, the straggle and the skewness determined by He on different configurations, as well as by different ion species. All these can be defined as the statistical moments for all ions stopped within the target window. Some of the results are shown in table 2.1.

Among the different stacking compositions, we considered one including a 2nm thick Si capping layer on top of MgB_2 (figure 2.4). The result showed that by adding the Si top layer, the ions are able to get deeper into the structure (more ion concentration inside the SiC substrate) and more vacancies are generated in our MgB_2 thin film. Since dealing with very thin layers, the difference is actually minimal and there are many possible reasons why we observe this results. First of all, the negligible observed increase in depth may be due to some generated interactions of the ions at the additional interface

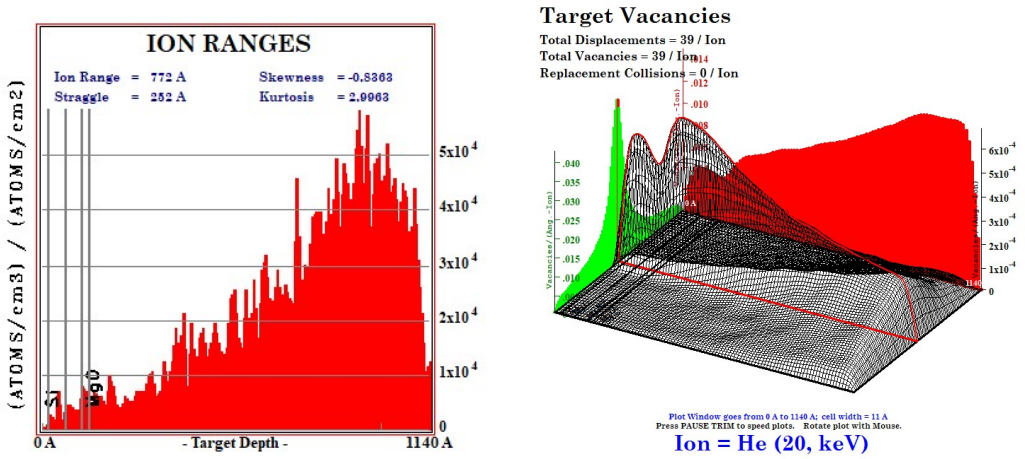

(a) (b)

Figure 2.4: Ion ranges and target vacancies generated by a 20 keV helium ions beam on the MgB_2 thin film covered by a Si capping layer. The obtained ion range is of 772 Å.

between Si and MgO. This may explain why, on the contrary, increasing the thickness of the Si layer, the number of vacancies increases as well. Moreover, it's important to notice that in the presented simulation, the crystalline structure of the materials is not taken into account and therefore neither possible channeling effects are (see chapter 2.2).
Concerning the results showed in table 2.1 and 2.2, they can be explained referring to the different phenomena may occur during the interaction. In particular, the stopping power of a target material for

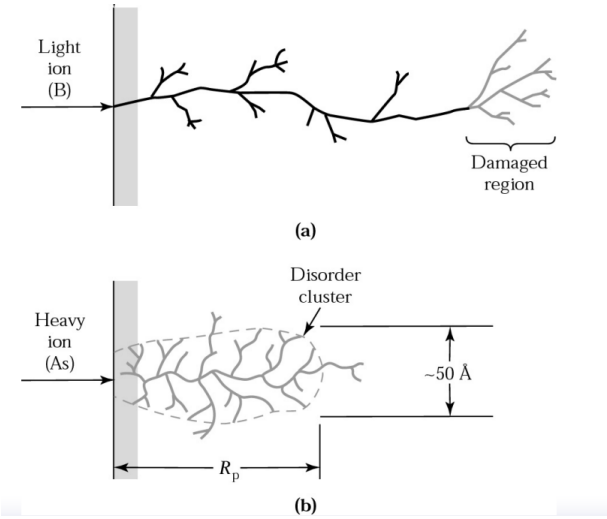

Figure 2.5: Implantation disorder caused by (a) light ions and (b) heavy ions (figure taken from [16]).

a striking ion is the loss of energy per unit of depth and it can be considered as the sum of nuclear and electronic contribution (nuclear elastic and electronic inelastic interactions are the only with practical effect for ion implantation). Of course, if the dose is high enough, the implanted layer will become amorphous and the heavier is the implanted ion, the lower will be the dose required to create an amorphous layer [17]. Indeed, what we would expect in terms of damage is that heavy ions will be immediately nuclear stopped, while light ions will first undergo a (high energy) electronic stopping and then a (low energy) nuclear stopping [18]. For instance, the investigated ion species for NbN are He, Ga and Ar (table 2.2) and, as expected, the heavier the impurity, the lower the dose that is required to create higher damage. Indeed, the ion ranges for Ga and Ar ion irradiation are similar and pretty much

He ions irradiation of 5 nm MgB_2 with Si capping layers.			
	20 keV	25 keV	30 keV
Ion range (Å)	772	628	599
Total vacancies	39/ion	20/ion	17/ion
Straggle (Å)	252	299	291
Skewness	-0.836	-0.122	-0.133

Table 2.3: Comparison between different irradiation energies of He ions onto a Si capped MgB_2 thin film.

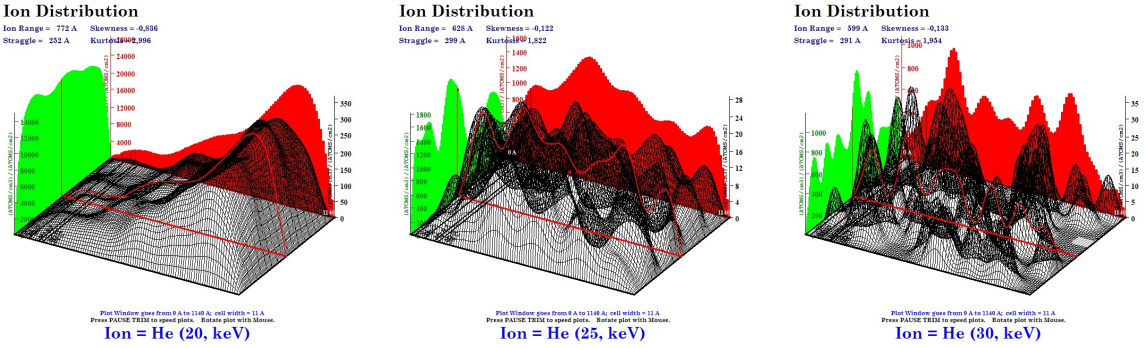

(a) **(b)** **(c)**

Figure 2.6: Interaction Helium ions at different acceleration voltages with MgB_2 Si capped layer.

separated from the He case. The first two, indeed, likely undergo a nuclear stopping while the light He ions penetrates easily into the material, leading consequently to a higher ion range. As a result, in the case of the manipulation of thin superconductive films ($\sim$ 5 nm), the light He ion is the best choice to allowed for the modification of the thin film properties (figure 2.5). Finally, we compared the results obtained by changing the acceleration voltage of the irradiated ion beam onto the target material, shown in 2.3.

As we can observe from figure 2.6, by increasing the energy of the exposed ions more and more He ions can actually be found into the thin MgB_2 film. Indeed, when dealing with higher energies, more interaction occur into the material and consequently an higher stopping power is expected, mostly caused by electronic stopping.

2.2 Channeling effect

For the understanding of the modified properties of our superconductive film under He irradiation, channeling effects should be also taken into account in the case of the crystalline MgB_2. Channeling effect is a phenomenon for which the implanted atoms in a material can follow a straight path through the crystal along certain lattice planes or directions, which are called "channels". Indeed, in a crystal layer there is a significant probability that the implanted ions trajectory is aligned with crystallographic planes of low Miller indices, i.e larger space. They result in a channel where ions are not subjected to nuclear scattering and the energy loss is mainly due to electronic interaction. In this condition, the interatomic potential itself contributes to keep the ion in the direction of the channel and the distance before the ion stop can be significantly larger then in the case of amorphous layer, resulting sometimes in a double increase of the implant depth. Of course, this phenomenon is strictly related to the crystalline MgB_2 case, while it would be only partially relevant in the polycrystalline NbN case.

What we expect in principle is that, when the ion beam is not in the direction aligned with crystal

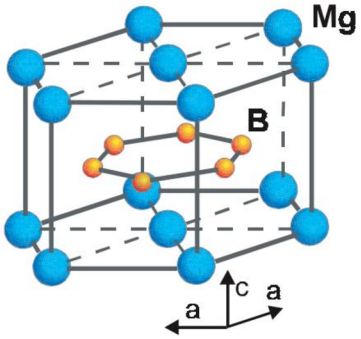

Figure 2.7: Magnesium diboride crystal structure [19].

channels, they will be able to stop before the end of the thin film. Actually, in the simulations above, the crystalline structure of the materials is not taken into account, since the SRIM simulation tool considers all the materials as amorphous. What we would expect from further experiments is that by twisting and/or tilting the ion beam (or similarly the stage of the sample) by an angle more ions will get into MgB_2. In figure 2.8, simulations with 0° and 8° has been shown, where no channel effects are accounted, so that they can be compared with future experimental results, in order to investigate the channeling effect and possible way to minimize it, whenever needed for our application. Moreover, as said before, the channeling effect could be a valid explanation for the obtained results when a Si capping layer is considered (see chapter 2.1). In particular, if in our simulation the ions appear to go further inside the target when the Si layer is applied, it is possible that this is just a consequence of the non considered channeling. Indeed, the capping should in principle diminish the propagation of the ions because of the additional layer with a different crystalline structure added. Furthermore, another possible reason why He ions seems to go deeper with the Si capping in our simulation can be attributed to different interfaces. Indeed, more interfaces could probably generate different changes in ion currents and consequently different channels [20].

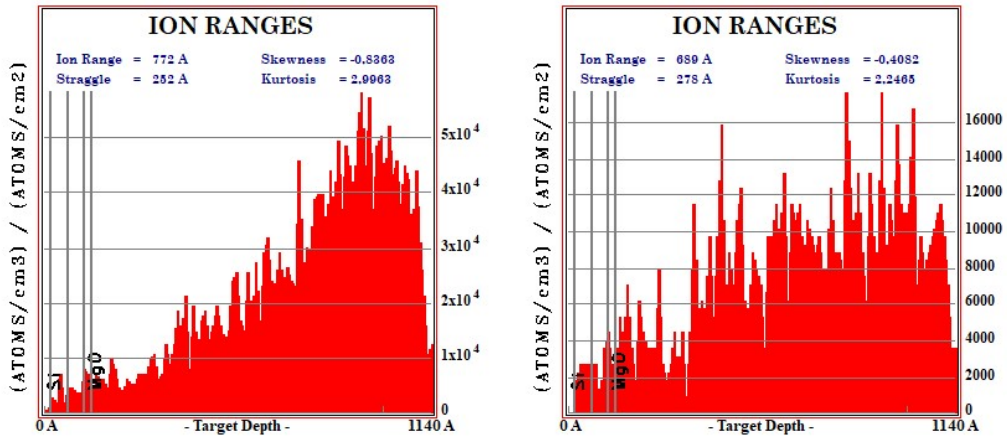

(a) **(b)**

Figure 2.8: Ion range comparison between 0° ans 8° tilted ion beam.

Chapter 3

Material and fabrication

Our MgB_2 samples consist of microwires of 1, 2, 3, 4, and 5 μm wide wires patterned on a $\sim$ 5 nm thick MgB_2 film on a 500 nm SiC substrate, with total active area in a range up to 400 x 400 μm^2. The NbN samples consist in two different layouts. We fabricated nanowires of 0.5 μm, 1 μm, 5 μm wide wires of $\sim$ 15 nm thick NbN film on a 300 nm SiO_2/Si substrate, designed mainly for dose tests and for the attempt to fabricate resistances. Moreover, NbN SNSPDs with a total active area of 10 x 10 μm^2, 8 x 8 μm^2, 5 x 5 μm^2 has been patterned in order to analyse the effects on the detector metrics (see figure 3.4).

3.1 Process flow

The two layouts used in our experiment has been designed by using PHIDL, an open-source GDS-based CAD tool for Python that extends Gdspy. In particular, the design has been created considering the properties of the different materials, namely, choosing a larger meander area and wider wires for the MgB_2 detectors.

3.1.1 Magnesium diboride

The MgB_2 thin film has been deposited through Hybrid Physical-Chemical Vacuum Deposition (HPCVD) and the microwires have been fabricated in the clean room.
Firstly, the samples have been rinsed into acetone and isopropyl alcohol (IPA) in order to remove particles and impurities from the surface and to improve adhesion and reproducibility. After this, the high-resolution positive e-beam resist (Zep530) has been spun on 4000 rpm for 4 minutes. Then, after baking the resist (180 °C for 2 minutes) to allow the partial evaporation of the solvents, the resist has been patterned with HS50 e-beam lithography by exposing at about 550 $\mu C/cm^3$ and developing in xylene for 60 seconds at 0°C and with IPA for 30 s at room temperature. After the fabrication, ion milling with Ar^+ at a beam voltage of 300 V for 15 minutes (1 min on and 2 min cool) and an angle of 30 degrees has been performed for the patter transfer. The obtained fill factor was of about 75%, i.e. the ratio of the active area to the total cross-sectional area of the nanowire.

3.1.2 Niobium nitride

The NbN thin film has been sputtered using an AJA Orion sputtering system for 390 s with a peak power of 140 W, which allowed the deposition of $\sim$ 15 nm NbN films.

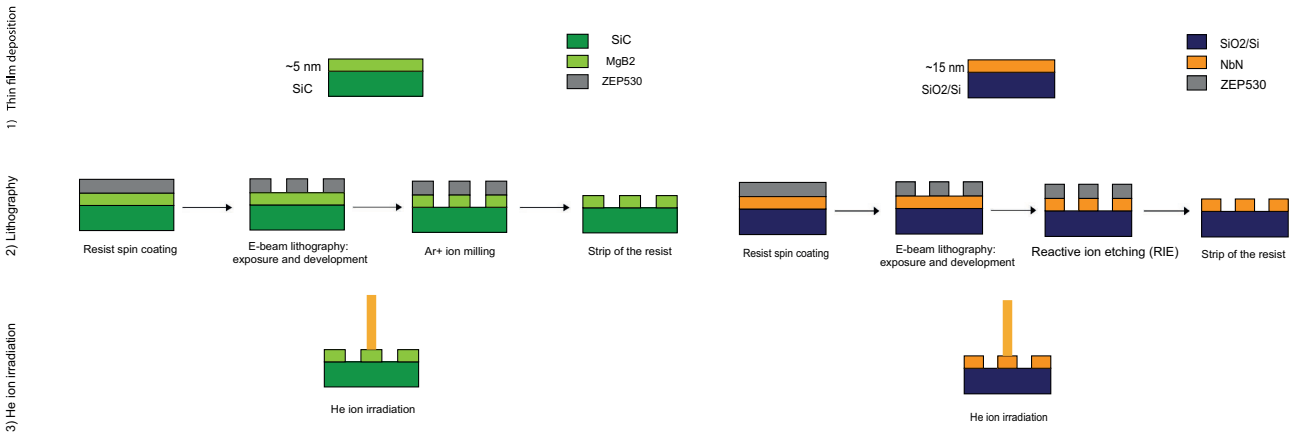

Figure 3.1: MgB_2 (left) and NbN (right) samples fabrication process flow.

After deposition, the thin film thicknesses were also measured using an ellipsometer. Similarly to before, after the samples have been cleaned, Zep530 was spun coated on the sample 5000 rpm for 60 seconds. Then, the samples has been baked at 100 °C for 120 seconds, aligned, exposed at about 550 $\mu C/cm^3$ and then developed in xylene for 60 seconds at 0°C and with IPA for 30 s at room temperature. A PlasmaTherm 790 reactive ion etcher (RIE) with CF4 at 50 W of power was used to transfer the patterns. Then the residual resist was removed with 1-methyl-2-pyrrolidone (NMP) at 70 °C for 1 hr.

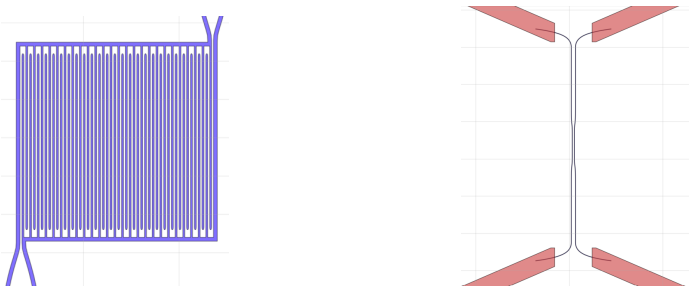

(a) **(b)**

Figure 3.2: SNSPDs (3.2a) and single nanowires (3.2b) layouts.

3.1.3 Helium ion exposure

After the fabrication, we irradiated the devices with He^+ using Zeiss Orion Microscope equipped with a Raith pattern generator. The irradiation was realized by sweeping the beam across the interested area. For the meander SNSPDs we irradiated all the active ares of the detector, while for the single nanowires we exposed in three different ways (see chapter 4.2.1).

The Gas Field Ion Source (GFIS) is the fundamental technology of this charged particle microscope, which is different from a conventional gallium FIB (Focused Ion Beam) or a conventional SEM (Scanning Electron Microscope). In this tool, the He^+ ion source consists of a very sharp tip ending with three atoms known as trimer. In order to have a good stability towards fluctuation (i.e. presence of impurities), the tip is cooled down up to 75 K. The tip can be biased with an acceleration voltage from 10 kV to 30 kV. At the center of the ion gun there is the gas field ion source (GFIS) which consist of a crystalline wire with a sharp end. Under the right conditions, the atoms at the apex will reorganize into a three sided pyramid which is atomically precise. When a voltage of about 30 kV is applied to the

emitter, a very high electric field will surround the apex of the needle, with the highest fields adjacent to the most protruding atoms of the emitter (fig 3.4). When neutral helium gas atoms are near this region, ionization occurs.
In particular, as shown in the simulation part (see chapter 2.1), higher implant acceleration voltage means more scattering with the target material, meaning that lowering it would lead probably to a higher concentration of ions into the thin superconducting layers (closer to the surface). Another important parameter in this tool is the current beam which can go from 0.1 pA to 10 pA and in order to obtain the highest possible current, different parameters has been taken into account:

- The aperture, the bigger available in the tool was chosen (20 μm);
- The trimer, the irradiation was performed more or less within few days after a new trimer had been created. This is, indeed, the best condition to get the highest possible beam current output, avoiding the deterioration and the contamination that can occur at the trimer even only one week after its formation;
- The helium pressure, being it directly proportional to the beam current.
- The spot control setting, which is a parameter that allows for the control of the strength of the condenser lens. Decreasing it means increasing the beam current and lowering the beam resolution.

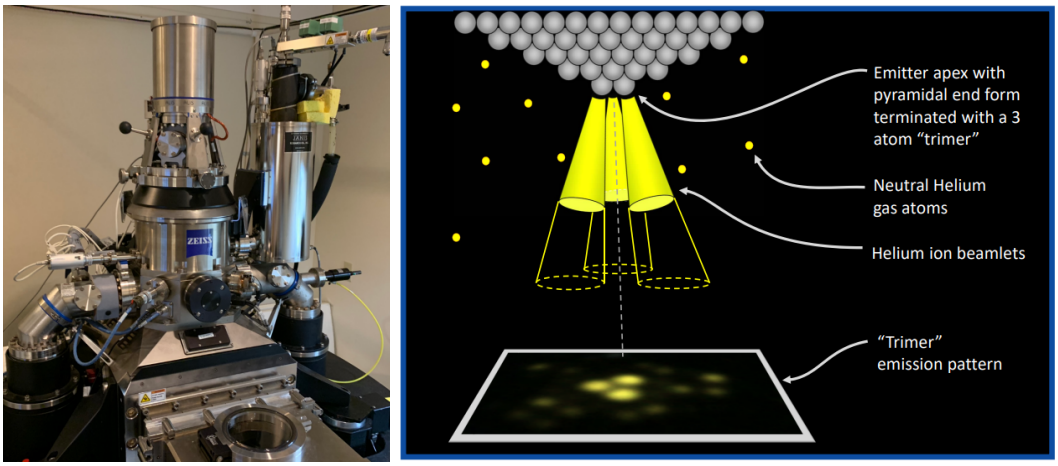

Figure 3.3: The Zeiss Orion Helium Ion Microscope. The apex of the emitter exhibits a classical faceted geometry under the right conditions. The end-form resembles a 3 sided pyramid with a very gradual slope. The ionization proceeds when neutral helium gas atoms pass into the regions adjacent to the most protruding (right figure taken from [21]).

Depending on the previous described parameters and on the geometry of the irradiated device, different exposure time where necessary to obtain the wanted dose. Concerning the fabricated SNSPDs with a meander shape, aiming to the modification of the SNSPDs detection properties without damaging them, we irradiated with a dose of $\sim 10^{14}$ ions/cm^2 the bigger MgB_2 ones and with a dose ranging from $\sim 10^{14}$ to 2.6 10^{17} ions/cm^2 for the NbN ones. For the single NbN nano and micro wires, we used a wider range of irradiation doses, from $\sim 10^{14}$ to $\sim 10^{20}$ ions/cm^2. An acceleration voltage of $\sim$ 30 keV and a current of $\sim$ 4 pA have been used.

3.2 SEM characterization

Scanning Electron Microscopy (SEM) technique has been used to characterize the samples before and after the He ion irradiation for both MgB_2 and NbN.
In general SEM is a powerful tool for characterizing the surface morphology, topography and the composition of samples. In our case the technique helped us to understand the influence on the materials of parameters such as fabrication process flow, electrical degradation and the helium ion irradiation.
Starting from MgB_2, in figure 3.5 we can observe the microwires before and after the ion irradiation.

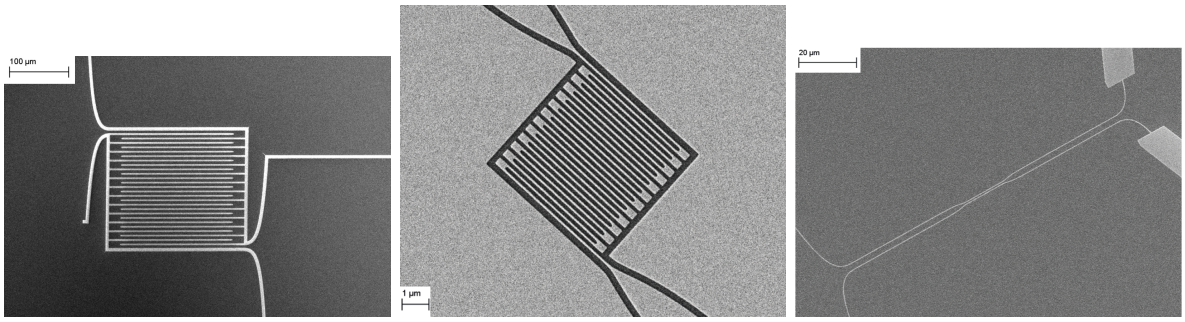

(a) **(b)** **(c)**

Figure 3.4: SEM of a) an MgB_2 meander microwire, b) a meander NbN nanowire and c) a NbN single nanowire before the irradiation.

Some spots were observed prior to irradiation. These spots may be attributed to various factors including the fabrication process, electrical measurements, and variations in cooldown procedures.
The presence of dark spots in the MgB_2 film is likely a result of material degradation or exposure to humidity, possibly due to the inadequate protection provided by the native oxide formed during post-ion milling. Our work on MgB_2 samples has revealed the delicate nature of this material, emphasizing its susceptibility to damage. Particularly, the oxidation process that may have occurred on the film is a phenomenon that deserves attention. Additionally, it is plausible to consider the association of these spots with issues related to the Ar^+ ion milling process. Indeed, achieving uniform etching depths and

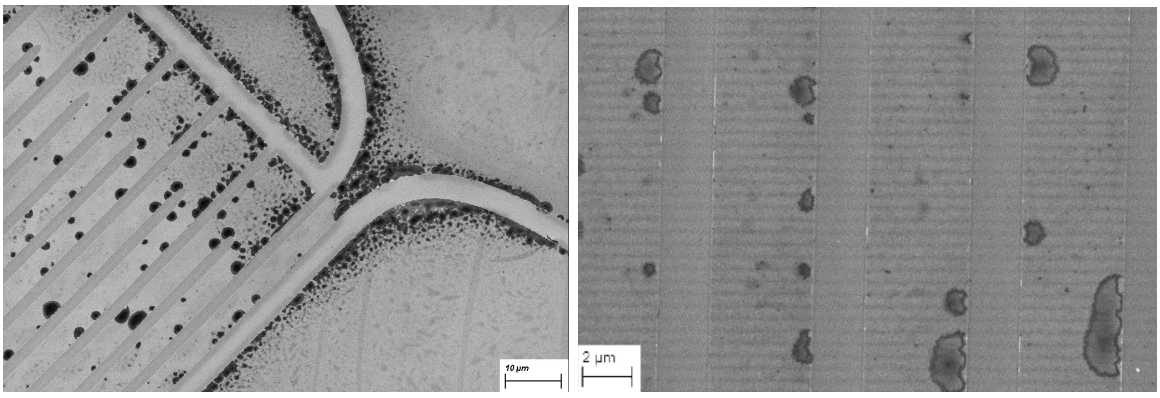

(a) **(b)**

Figure 3.5: MgB_2 micro-wire after electrical measurements (3.5a) and after the irradiation (3.5b).

preventing surface contamination can be challenging with Ar^+ ion milling. The observed spots could potentially be remnants of resist, but a thorough investigation through energy dispersive spectroscopy (EDS) analysis is necessary to determine their nature.

The same images have been taken after the He irradiation aiming to identify any visible effects, such as damages, caused by the ions on our micro-wires. It is important to note that the doses used for irradiating our MgB_2 micro-wires are in the range of 10^{14} ions/cm^2. The impact on the superconducting thin film is likely to involve modifications in the crystalline structure and visible damage (3.5). However, at low doses, the superconductivity is not expected to be completely destroyed. This could explain why we do not observe any clear and evident damage to the material. In figure 3.6, the scanning electron

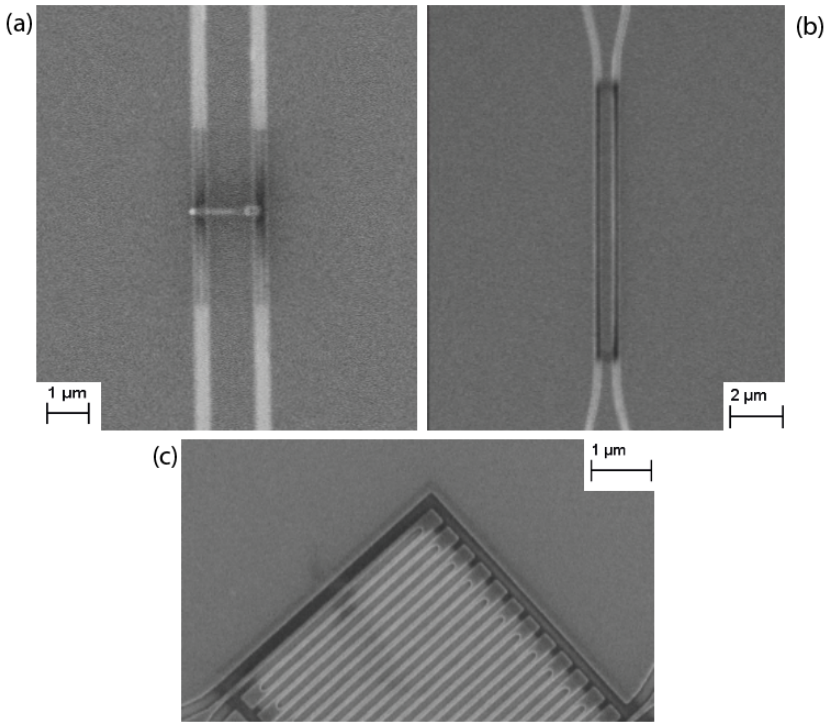

Figure 3.6: NbN devices after the helium ion irradiation.

microscopy images of the NbN single nanowires and of the SNSPDs after irradiation are presented. The impact of helium ions varied depending on the applied dose. Notably, at higher doses, visible damage was generated in the material.

Chapter 4

Electrical and optical measurement

4.1 Magnesium diboride

In this section, we investigate the results obtained from our high-T_c superconducting MgB_2 microwires, investigating measurement apparatus and comparing them before and after the helium irradiation, with focus on the hysteric I-V curve and on the basic detector metrics. A pulse tube cryostat was used in this experiment, which allows for a standard temperature of operation of $\sim 3.8K$ and of which main components are a compressor, a cold head, a heat exchanger, and a regenerator. This cryostat allows to get very fast different measurements at different operation temperatures to get easily transition curves. After the devices were wirebonded on a particular PCB, we inserted our sample in the chamber, where

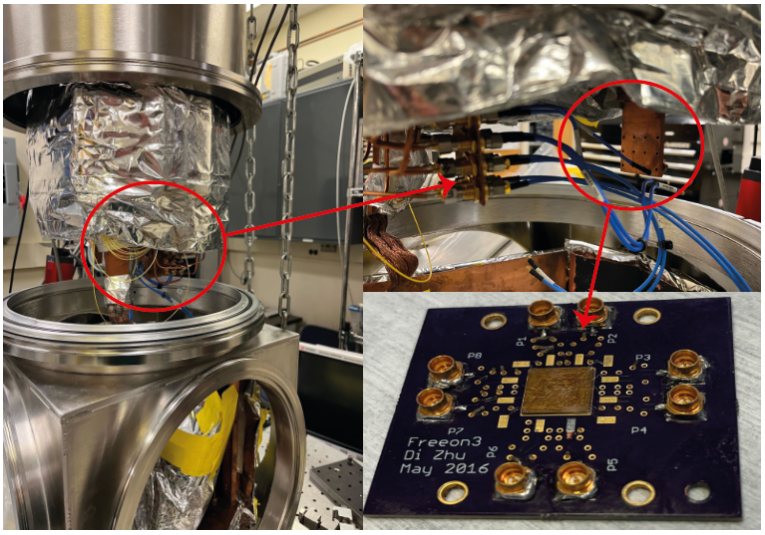

Figure 4.1: On the left, the pulse tube cryostat used for this experiment. The top right image shows the sample holder and the bottom right shows the PCB where the chip has been wirebonded.

the vacuum was created.
The measurement setup consists of a voltage source obtained by applying a 10 kΩ resistor to a tester, i.e. the voltage source, a multimeter and a parallel resistance of 1 MΩ in order to inhibit the current flow in the last. A two point contact was used here, since there was no need to eliminate the contact resistances with a 4 contact measurement.

From the I-V characteristic of our MgB_2 samples is the theoretical value of the critical temperature as well as how it varies during the cooldown can be obtained. Moreover, the sensitivity of the nanowires to light has been studied through dark and light count measurements and the response to the laser

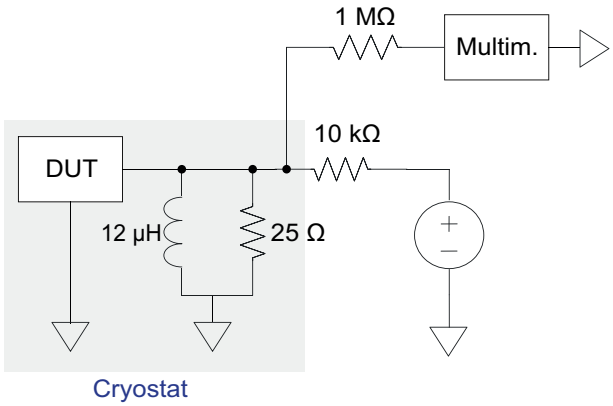

Figure 4.2: Circuit for the electrical measurement. A shunt inductor (12 μH) has been used.

radiation has been investigated before and after the He irradiation on the microwires. Even before the irradiation, the most important result has been obtained for the 5 μm and 4 μm wide wires, which turned out to be the only one to superconduct. Indeed, in the case of our MgB_2 microwires, a fill factor of 75 % would probably be too high and let some current crowding into the material, meaning that the superconducting current becomes higher than the critical current density, causing a breakdown of superconductivity in localized regions. From a subsequent analysis it turns out that a fill factor of 50% or a gap 15% higher than the wire would be proper in order to avoid it.
We proceed with two pumpdowns with different apparatus, undertaking many thermal cycles. While the first pumpdown had simply the sample chip at the cold stage, the second one additionally had a combined shunt inductor/resistor at the cold stage (see figure 4.2).
Starting from the first cold down, DC measurements were taken with and without a room-temperature

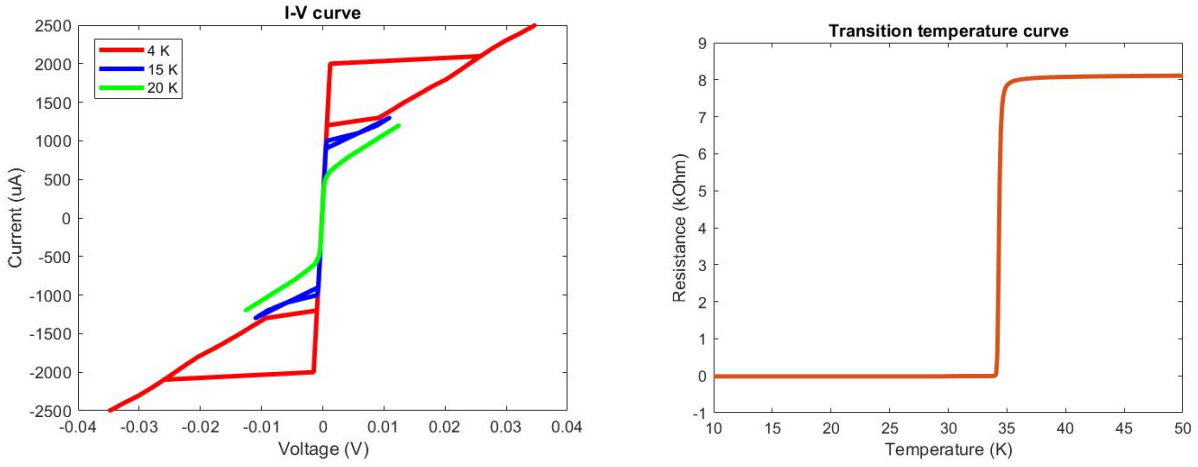

(a) **(b)**

Figure 4.3: I-V curves (4.3a) and transition temperature curve (4.3b) for the 4 μm wide wire without the shunt inductor.

shunt. What we observed is that the shunt inductor at the warm stage was not able to prevent latching, the condition in which the SNSPD remains in the normal resistive state even after the incident photon has been absorbed and the energy has been dissipated. For example, for the 4 μm wide wire, the switching current was found to be of 2 mA at 4 K and the retrapping current 1 mA indicating a wide and sharp hysteresis. The highest temperature at which the hysteresis is strongly observed is 15 K,

when the switching current is 1 mA and the retrapping current is lowered. At 20 K no more hysteresis is visible, i.e. a consequence of the transition between the superconducting and normal states of the nanowire, and the wire still exhibits superconducting behavior with a switching current of about 0.8 mA (see figure 4.3).
Moreover, in figure 4.3 we can observe the typical superconducting transition curve without the shunt inductor, where T_c is about 34 K, defined to be the temperature where the resistance drops to 50% $R_{40}K$ and a sheet resistance of 4 kΩ. The transition width (ΔT_c), defined as temperature width between 90% and 10% R_{40K}, resulted to be around 1.5 K.
With the second cooldown, considering the shunt inductor configuration, the switching current lowered

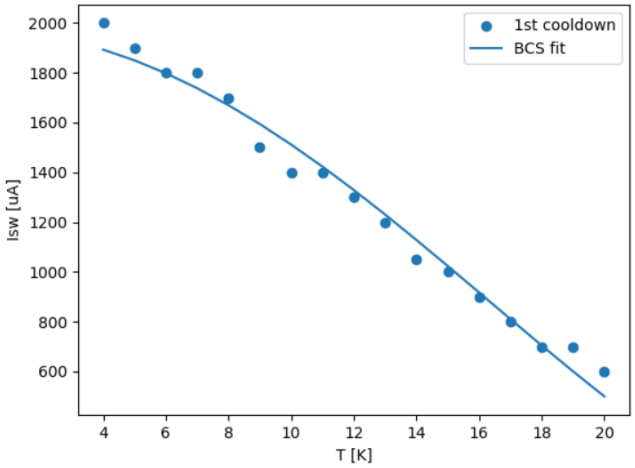

Figure 4.4: Switching current as a function of the temperature.

significantly up to 400 μA and with a trend coherent with the previous one (figure 4.4). Subsequently,

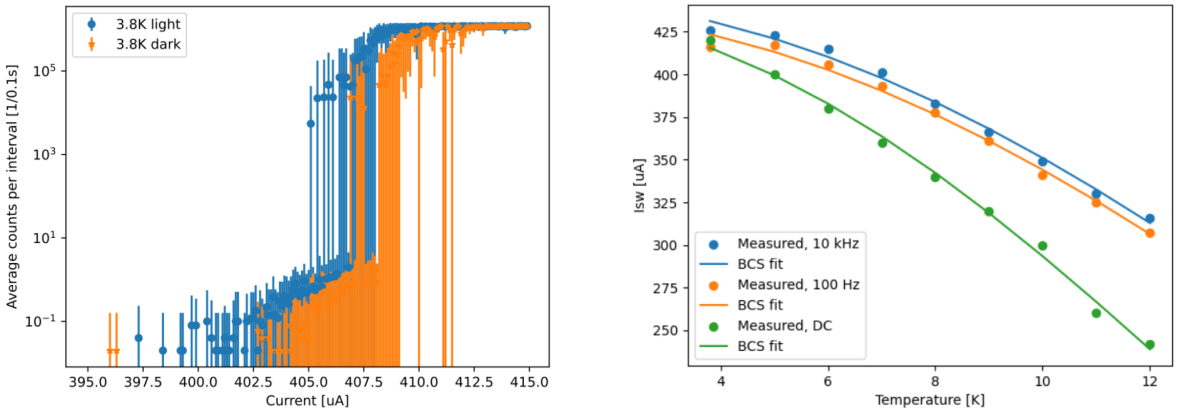

(a) **(b)**

Figure 4.5: Detector sensitivity analysis. Fig. 4.5a dark and light count curves at 7 K. Dots and lines represent respectively the average counts per interval and the uncertainty.Fig. 4.5b: comparison of DC, 100 Hz and 10 kHz measurements.

we investigated the sensitivity of our SNSPDs to light during both the first and second cooldown. Lasers of 1550 nm and 780 nm were used. In particular, with the shunt inductor we succeded in preventing latching but even if a pulsing behavior was observed up to 14 K, these can not be associated with light counts. Indeed, what we observed is that the coupling to laser light caused a switching current

suppression of only 2 μA at all temperatures where hysteresis was seen. Additionally, the dark and light count curves at a given temperature were found to be statistically identical and just shifted by a value of 2 μA (figure 4.6). What we expect is to obtain a higher sensitivity after the He ion irradiation. Finally, detailed switching statistics were taken with an arbitrary wave generator (AWG) and an oscilloscope. In the case of 100 Hz and 10 kHz measurements indicated significantly higher switching currents than of the DC case are obtained, especially at higher temperatures, which cam be attributed to the ability of filtering out noise at higher frequencies (figure 4.6).
After the irradiation of the entire meander of the MgB_2 microwires we repeated the same measurements of before. After the ion exposure, the switching current measurements indicated an open circuit condition, probably caused by some mechanical damage occurred on the material. In particular, the

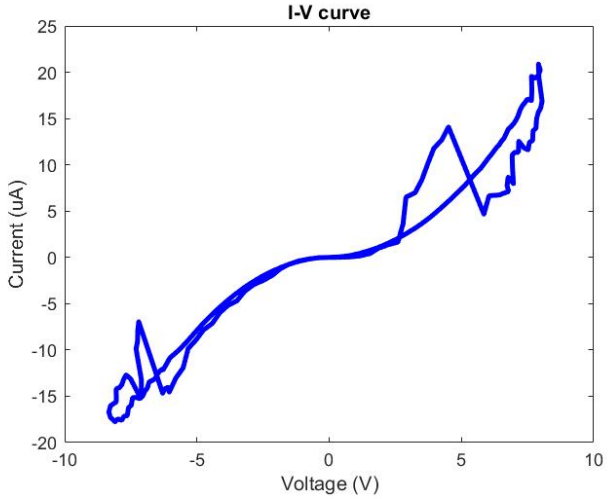

Figure 4.6: I-V curve after the helium irradiation at $\sim$ 7K.

5 μm wide-wires showed a semiconductive/insulating behaviour and a room temperature resistances which changed from $\sim$ 10 kΩ to $\sim$ 10 MΩ. Considering the fragile nature of MgB_2, it's unclear whether this results come from the irradiation or from some environmental exposure. We intend to investigate this further in the future.

4.2 Niobium Nitride

In this section, an overview of the relevant experimental observations of the effects of helium ion irradiation for SNPDs will be described. Our results are very promising for applications such as detector post-processing, high temperature SNSPDs and possibility of direct fabrication of functional elements (bias resistors).

4.2.1 Single nanowires

Starting from the single nanowires, we performed I-V measurements in order to investigate the effect of helium irradiation. In this experiment a liquid helium dewar was used which allowed us to operate at 4.2 K. In particular, the samples were inserted into the dewar thanks to a custom-built dipstick probe provided with 28 RF connection lines to measure 28 device per cool down, a temperature sensor and an optical fiber. Before mounting them, the samples have been wirebonded over a specific PCB with

Figure 4.7: On the left, the dipstick probe inserted into the liquid helium dewar. The top right image shows the tip used to wirebond the chip. The bottom right shows the PCB mounted on the probe. Our NbN samples were placed in the middle of a PCB with 28 contact pads for the connections and 0 Ω soldered resistors.

28 contact pads (figure 4.7). Different kind of irradiation at all the different doses has been performed to the nanowires: an irradiation over two squares on the wire (fig. 4.9); the irradiation of the entire smaller wire (fig. 4.8); just a bridge-like cut, i.e. just a line perpendicular to the wires (fig. 4.9). The

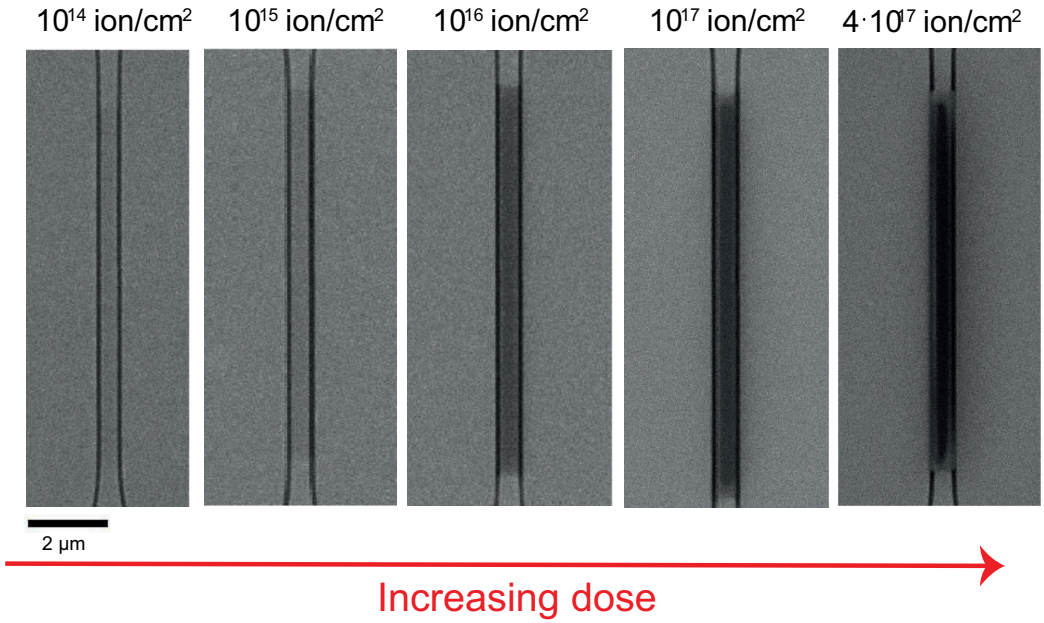

Figure 4.8: Imagines taken with the helium irradiation tool. Irradiation with increasing dose over the entire nanowires.

critical current measurements has been done with a simple electrical setup shown in figure 4.10. A DC bias voltage and a 10 kΩ resistor has been applied. The measurements has been performed both with a Keithley 2700 digital multimeter and a Lecroy620zi oscilloscope. The current over the device is defined as:

$$I_d = \frac{V_B - V_D}{R} \tag{4.1}$$

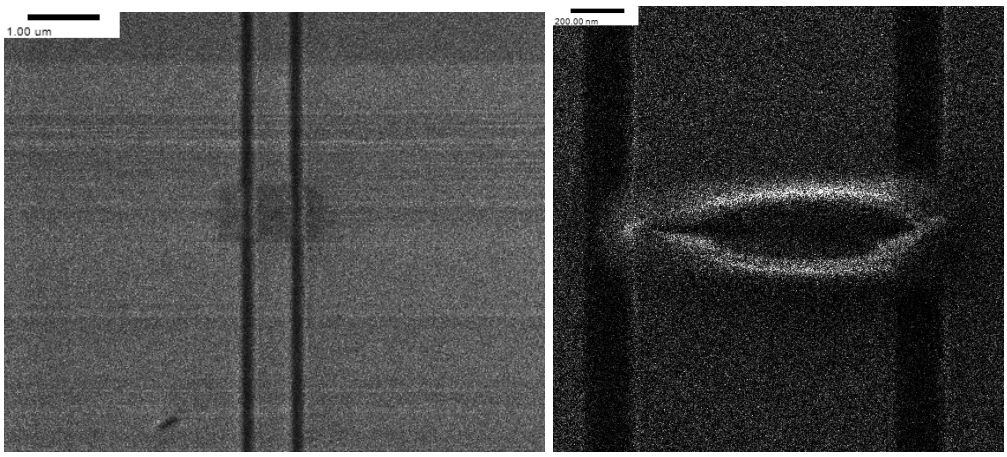

(a) **(b)**

Figure 4.9: Imagines taken with the helium irradiation tool. Fig. 4.9a: irradiation of two squares on the wire ($5 \cdot 10^{16}$ ion/cm^2). Fig. 4.9b: irradiation of a single cut (10^{20} ion/cm^2).

where V_B is the bias voltage, V_D the voltage on the device and R the 10 kΩ applied resistor. The I-V

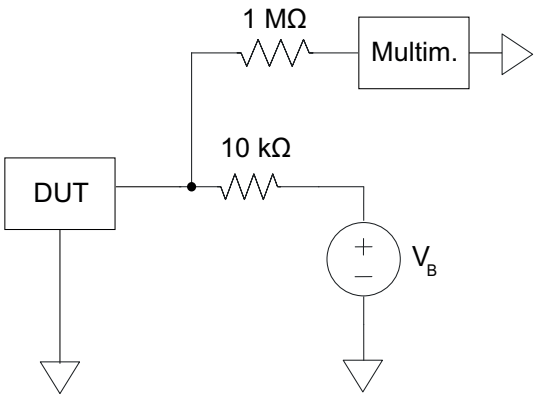

Figure 4.10: Electrical circuit for the critical current measurement.

curve has been obtained for all the device with the different helium dose, illustrated in the following. Several key observations can be made based on the experimental results. Firstly, the switching current, i.e the current threshold that identifies the transition from the superconducting to the normal state, is decreasing when the helium irradiation dose is increased. Moreover, the typical hysteretic behaviour, i.e the device remaining normal even at currents less than the switching one, is preserved until very high doses are reached. This hysteresis is due to self heating of the device when it is in the resistive state [22]. Indeed, the retrapping current, which is the minimum current required to return from the resistive state back to the superconducting state, remains more or less the same. In particular, coherent results can be observed in the three kind of irradiation performed. For the two square irradiation, the switching current is starting to notably decrease at a dose 10^{19} ion/cm^2, passing from $\sim$ 300 µA of the non irradiated case to $\sim$ 28 µA. In the range between $\sim 10^{15}$ ion/cm^2 and 10^{18} ion/cm^2 only a minimal decrease of the switching current is observed (figure 4.8). In the case of the completely irradiated wires, lower doses have been chosen, and the trend shows a bigger decrease of the switching current, relatively to the non irradiated wire, starting from a dose of 10^{15} ion/cm^2, after which it stays more or less the same up to another decrease at $\sim 10^{18}$ ion/cm^2 (figure 4.12). In accordance with the previous statement, in figure 4.13 we show the I-V curve and the relationship between the

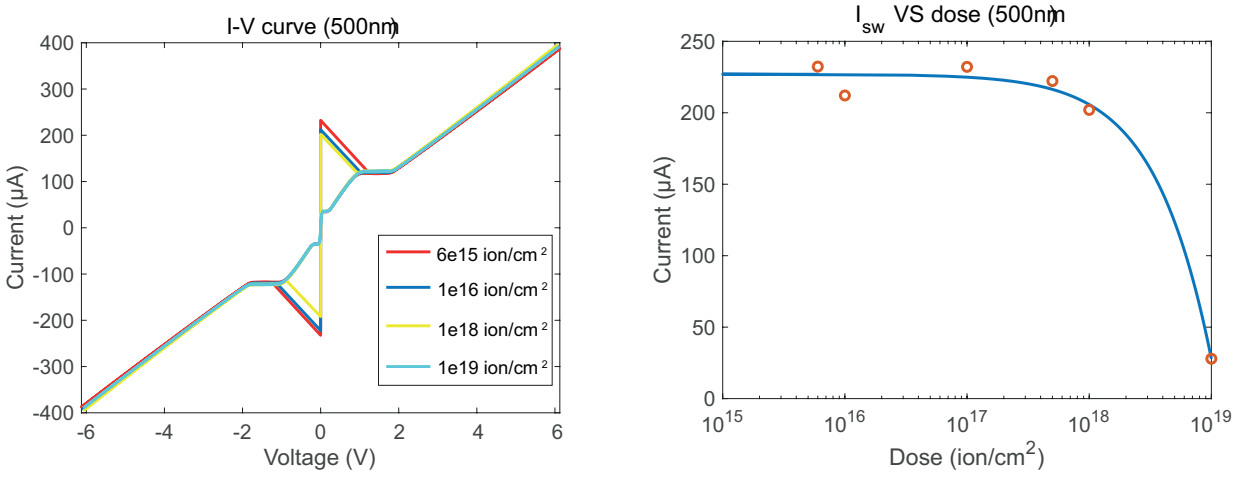

(a) **(b)**

Figure 4.11: Fig. 4.11a: current-voltage relation at different doses for the 500 nm wide wires, irradiated over two squares. Fig. 4.11b: relation between switching current and dose.

current and the dose in the one micrometer wide wire. In this case, the irradiation has been performed over a small perpendicular line on the wire. In this case, the switching current is decreasing from 800 μA to 600 μA from the non irradiated case to a dose of $\sim 10^{15}$ ion/cm^2. Then, as before, the decrease is slowed down until significantly decreasing again from a dose of $\sim 10^{19}$ ion/cm^2, reaching a value of $\sim$ 59 μA. We suppose that, at this high doses, the irradiation is starting to be efficiently destroying the superconductivity. Indeed, in this case, the retrapping current seems to be the same of the switching because no superconducting state is retrieve after the first switch. A resistance is created correspondent to the cut done with the helium ions and only the rest of the wire switched (at $\sim$ 60 μA). The resistance obtained has been extracted from the plot and result to be 1.8 kΩ near the helium irradiated bridge and $\sim$13 kΩ for the normal state of the rest of the wire. This is a very interesting result. Indeed, even if with the smaller possible irradiation area we were able to obtain a high resistance, the perspective of being able to tune this resistance with the different helium dose opens possibility towards fabrication of bias resistors. Moreover, in this experiment we already started with the high resistive NbN samples, meaning that interesting results could be obtained in the future with other materials, for example MgB_2. Eventually, in terms of change in the switching current, from our results we can deduce that for low doses, there is no difference with respect to the irradiated area over the wire (figure 4.15). On the contrary, when an high irradiation dose is applied ($\sim 10^{20}$ ion/cm^2), the device was completely destroyed in the case of the two square irradiated area while an additional resistive state was retrieved in the single cut case.

Overall, this experimental result suggest that the irradiated helium ions into the superconducting film is slightly modifying the properties for lower doses and eventually starting to suppress the superconductivity at $\sim 10^{20}$ ion/cm^2. Actually, several plausible explanations can be considered for this outcome. First of all, the switching current for a uniform nanowire and no external noise, should be equal to the Ginzburg-Landau depairing critical current of the device [23]). So in this case, the reduction of the switching current could be associated to a reduction of the critical temperature (of $\sim$ 6.5 K) due to the helium ions impinged onto the superconductive film, being the last already demonstrated for other materials. But in real measurements, the switching current can be $\sim$10% below the actual critical current, depending on the device kinetic inductance and the RF resistance of the readout circuit [24].

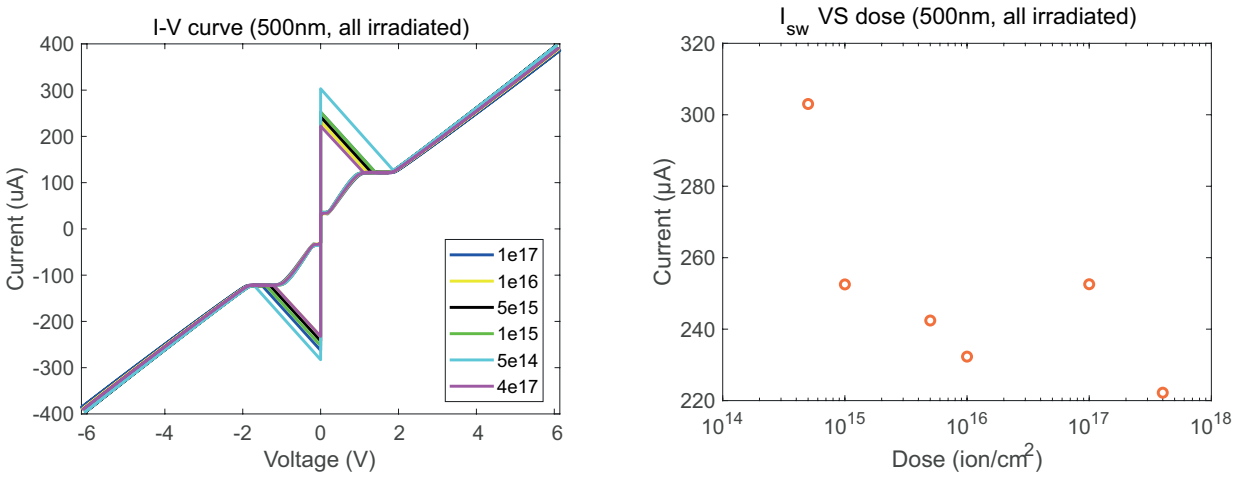

(a) **(b)**

Figure 4.12: Fig. 4.12a: current-voltage relation at different doses for the 500 nm wide wires, irradiated over the entire wire. Fig. 4.12b: relation between switching current and dose. At this low doses the decrease of the switching current is negligible.

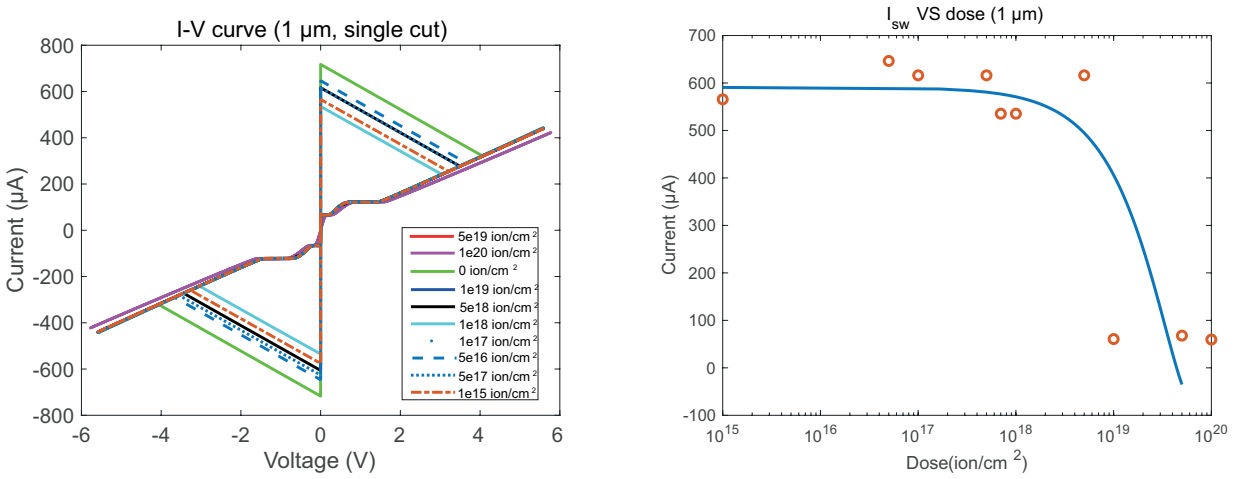

(a) **(b)**

Figure 4.13: Fig 4.13a: current-voltage relation at different doses for the 1 μm wide wires, only a single cut of helium irradiation has been performed. Fig. 4.13b: relation between switching current and dose.

This means that, the reduction of the switching current may be interpreted in terms of increase of the kinetic inductance and of the sheet resistance and so of the reset time (see chapter 3). Strohauer et al. also propose a model to describe the increase of the sheet resistance as a function of the dose:

$$R_{sheet}(F) = \frac{1}{v_D(1-(1-n_{D,0}v_D))} \cdot \exp(-\eta v_D^{2/3} F) \cdot \frac{a_{d0}}{d} \tag{4.2}$$

where v_D is the average cluster volume, η the efficiency in creating defects, F the ion fluency, $n_{D,0}$ the defect density of the non-irradiated film, a_{d0} a thickness dependent constant and d the film thickness. Indeed, an increase of the sheet resistance with the helium ions dose has been experimentally demonstrated in NbTiN [14], which gives support to our trend of decreasing current.
On the other hand, an other important point to be underlined here is that the current needed to restore the superconductivity (retrapping) has not been changed by the irradiation. This means that

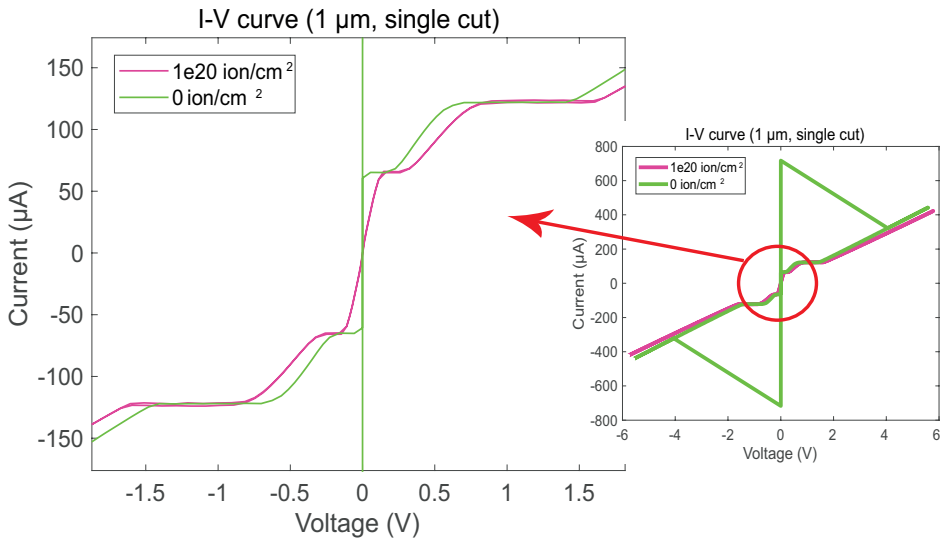

Figure 4.14: Comparison of the current-voltage relation between the 1 mu$m$ wide wires without irradiation and with a single cut of helium irradiation at 10^{20} ion/cm^2.

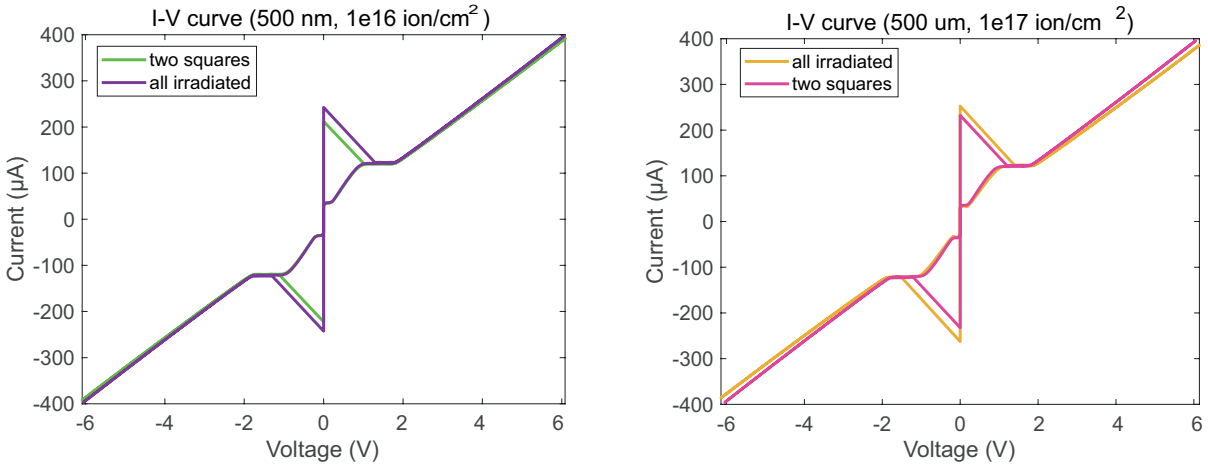

(a) **(b)**

Figure 4.15: Comparison between current-voltage relation at different doses for different irradiation on the 500 nm wide wires,i.e. entire wire and two squares irradiation.

the helium ions are probably not changing the cooling capacity of the nanowire after the generation of the hotspot and that the amount of Joule heating that the wire is able to dissipate at the measurement temperature (4.2 K) has not changed.
Concerning the destruction of the superconductivity when higher dose are applied, it's plausible that the high number of implanted ions inside the superconductor generates an average defect volume compatible or higher than the grain boundaries of the policrystalline NbN, changing it's structure and reducing the superconducting gap creating some kind of crossover.

4.2.2 Superconducting nanowires single photon detectors

In this section, we investigate the results obtained from the irradiation of the fabricated NbN SNSPDs in a meander shape with a total active area of 5 x 5 µm^2. For this devices, we selected lower doses ranging from $\sim 10^{14}$ ion/cm^2 and $\sim 2.6 \cdot 10^{17}$ ion/cm^2, to be sure not to irradiate up to the destruction

of the superconductivity, and we irradiated the entire active area. Firstly, we have used the same setup of before to obtain the current-voltage relationship on the different devices. In figure 4.16, we can observe a comparison of the I-V curve for the irradiated and non irradiated meanders. Firstly, the results are coherent with the single nanowires experiment: the critical current is decreasing when helium is irradiated, even if this decrease is relevant only with respect to the non irradiated case. Indeed, the switching current of devices irradiated in the range between $\sim 10^{14}$ ion/cm^2 and $\sim 10^{16}$ ion/cm^2 show only a minor decrease, which starts to become significant at a dose of $\sim 10^{17}$ion/cm^2.

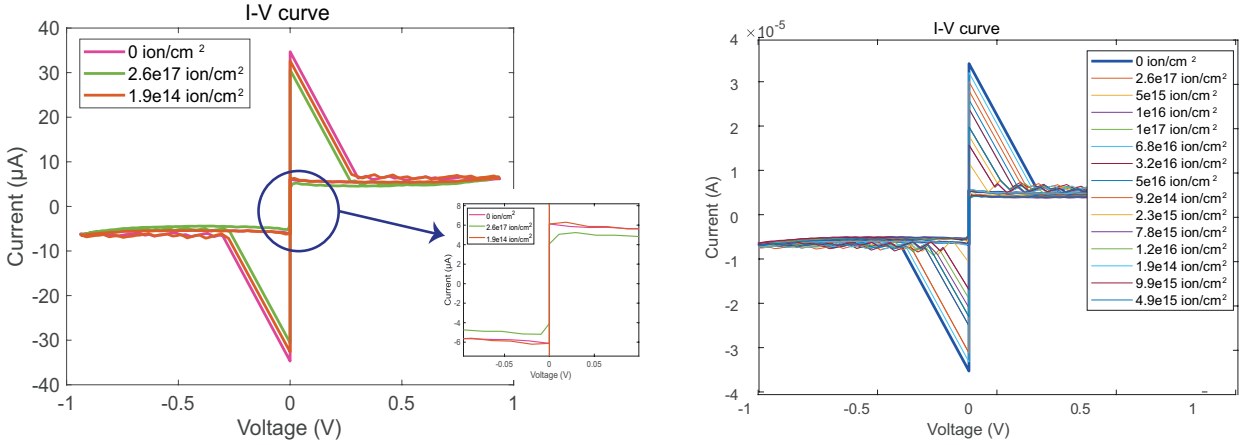

(a) **(b)**

Figure 4.16: Current-voltage relation at different doses for the 5x5 µm^2 SNSPDs, 100 nm wide wires.

Moreover, it is worth noting that in this case, in the device with the highest irradiation dose of 2.6$\cdot$ 10^{17} ion/cm^2, the retrapping current is reduced from 6.1 µA of the non irradiated device to 4.1 µA.
We will now focus on one of the main important metrics of SNSPDs: the detection efficiency. In literature, there are different accepted definition of detection efficiency. In general, single-photon detectors should be able to detect individual, randomly arriving photons and its efficiency can be defined as the number of individually measured events that are triggered by single-photons divided by the total number of photons incident on the detector:

$$\text{SDE} = \frac{\text{LPC - DPC}}{\text{PR}} \tag{4.3}$$

where LPC represent the photon count rate, DPC the dark count rate and PR the total photon rate incident to the probe station. The detection efficiency depends on the wavelength and generally is lower for more less energetic photons (higher wavelength).
In our experiment, we determined the count rate of our devices to discover if a detection improvement was obtained with the helium irradiation. The experimental setup consists once again in a liquid helium dewar and a dipstick probe (see figure 4.7) and the used electrical apparatus is represented in figure 4.17. A fiber-integrated laser of 780 nm has been connected to our dipstick probe and shined onto our detectors at a distance of about 2 cm from the PCB, allowing a flood laser illumination. A range between 0.03 and 4.8 mW of laser power has been used.
In general, the count rate of a single-photon detector is the number of single-photons detected per unit time, while dark counts can be defined as 'false' measured events that are indistinguishable from real detection events caused by incident single-photons.

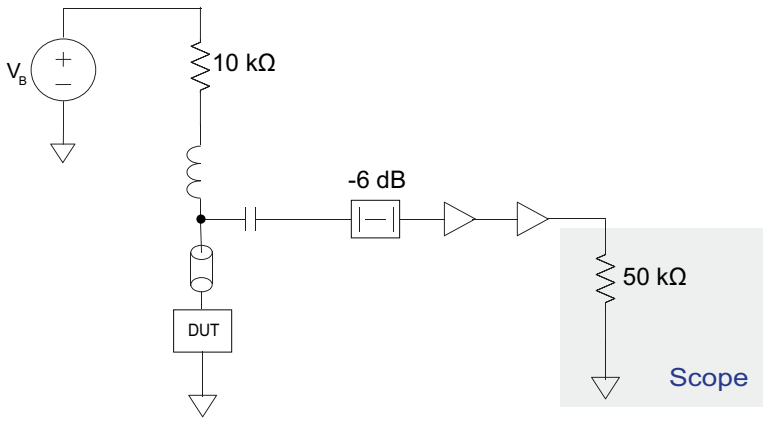

Figure 4.17: Electrical circuit for the photon count rate measurement.

In figure 4.18, we can observe the comparison of the LPC-DPC for the different devices and a laser

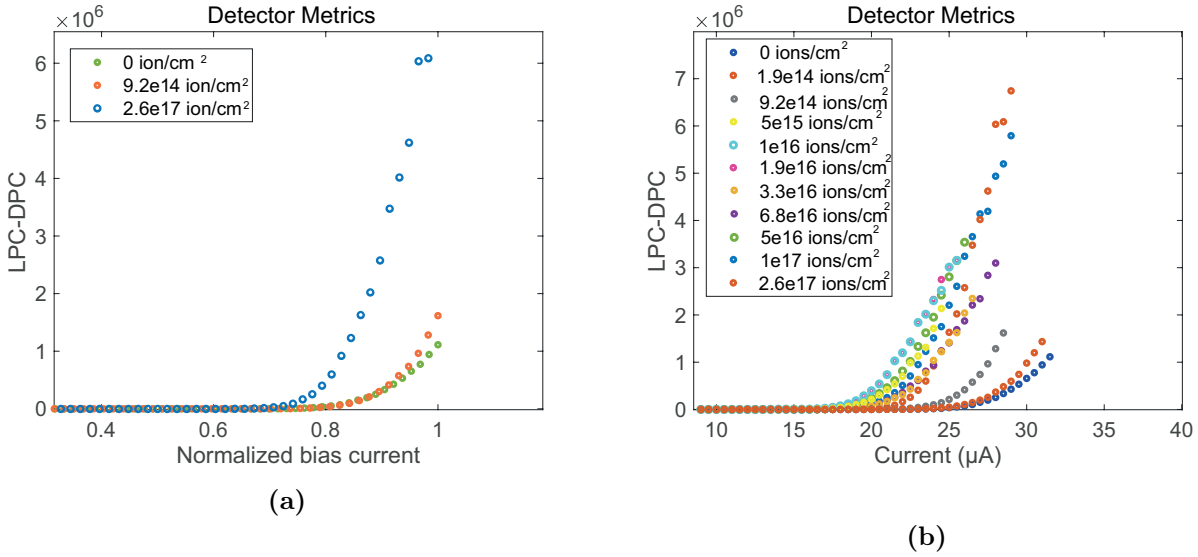

Figure 4.18: Photon counts vs current comparison for the different irradiated devices. A laser in the 780 nm wavelenght and power of 1mW has been used.

power of 1 mW. The results demonstrate strong potential and promising prospects: the most irradiated device shows an improvement in the detection ability with respect to the low and not irradiated ones. Specifically, a first significant improvement is recognizable for doses of around 10^{16} ion/cm^2, becoming more relevant at $2.6 \cdot 10^{17}$ ion/cm^2. Moreover, for a good detector both high detection efficiency and switching currents are desired. In this results, among this range of irradiation it seems that the switching current is not decreasing too much but the efficiency is increasing. This improvement in the detectors can be the consequence of different phenomena. First of all, it is worth remembering that the count rate is typically set by the reset time. In principle, for detectors with the same thickness and width the kinetic inductance and the reset time should increase with the helium irradiation dose due to the increase of the sheet resistance [14]. It is probable that in our case this increase of the reset time is compensated by the big thickness of the film (see equation 2.4). This means that, in order to understand the possible reasons why the detection seems to be improved by the helium ions irradiation, the different contributions to the system detection efficiency should be analysed. The last

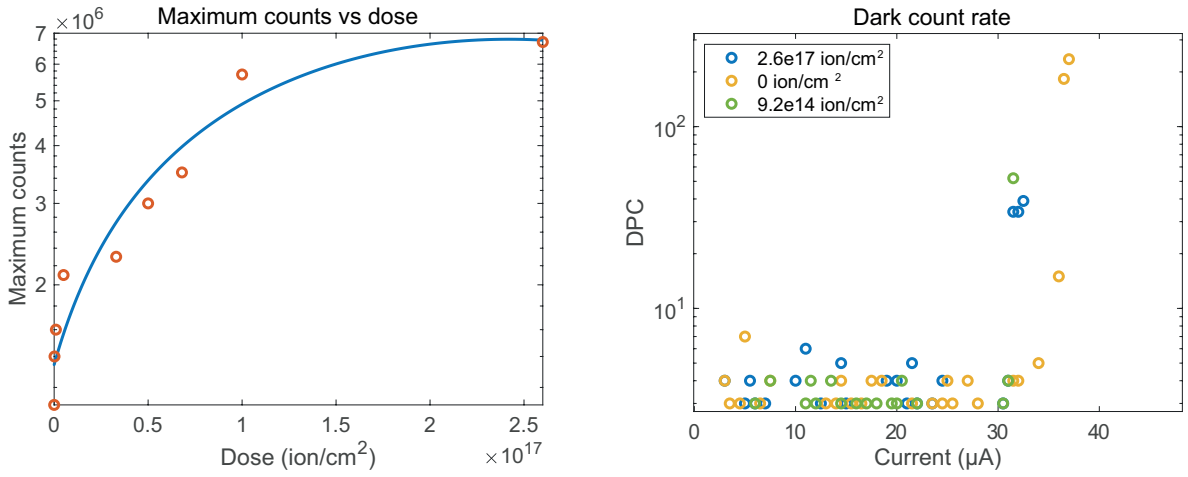

(a) **(b)**

Figure 4.19: Fig, 4.19a: maximum counts vs helium ion applied dose. An increasing trend can be observed. Fig 4.19b: comparison of the dark count rate for different SNSPDs.

has been defined by Natarajan et al. as:

$$\eta_{SDE} = \eta_{coupling} \cdot \eta_{absorption} \cdot \eta_{registering} \tag{4.4}$$

where $\eta_{coupling}$ is dependent on the loss of photons due to absorption, scattering or reflection within the experimental environment, $\eta_{absorption}$ due to the detector material and geometry and $\eta_{registering}$ due to the non-unity probability that the detector generates an output electrical signal after photon absorption. The value $\eta_{absorption} \cdot \eta_{registering}$ is defined as intrinsic detection efficiency. If the observed increase of the effective count in our irradiated detectors is due to an increase of the $\eta_{absorption}$ or $\eta_{registering}$ is difficult to deduce. In principle, it has been reported that in order to increase the $\eta_{absorption}$ a long interaction length for the incident photons is be needed, while the enhancement of the $\eta_{registering}$ has been observed for smaller size of superconducting energy gap which leads to an increased hotspot size for a given photon energy [25]. This means that is possible that the helium ions inside the polycristalline structure of NbN generate an enhanced absorption at the considered wavelengths or a reduction of the superconducting energy gap. Additionally, constrictions in the nanowire are possible limits for the intrinsic detection efficiency, since they do not allow the detector to be biased at a high current, lowering $\eta_{registering}$ [25]. It is possible that the helium ions are somehow lowering the effect of the constrictions, uniforming over the active area of the device.
Furthermore, a comparison of the obtained maximum values of LCR-DCR at different laser power has been provided (figure 4.20). Of course, increasing the laser power, more count will be detected by the same device. What is interesting is that, while the maximum value of counts in the non irradiated device depends negligibly from the laser power, the irradiated device show an increase of counts with the laser power. In the future, more characterizations and tests should be done to understand the origin of the described results. Another important consideration is that our SNSPDs don't get sufficiently high incident photon arrival rates to enter in the so called saturation region, i.e. after when the detector is will not be able to detect any addition single-photon. One must bear in mind that our fabricated SNSPDs are 15 nm thick and with a fill factor of $\sim$ 50 %. In the future it would be intriguing to investigate the possibility of perform the same experiment on already saturating detector and delve

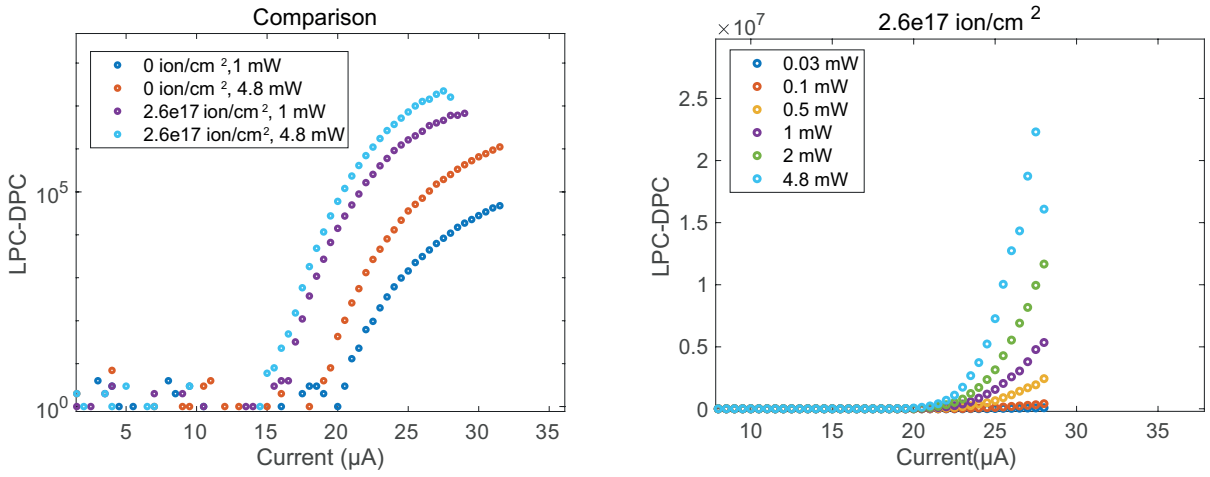

(a) **(b)**

Figure 4.20: Fig. 4.20a: photon counts vs current comparison for the different irradiated devices with a laser power of 1mW and 4.8 mW. Fig. 4.20b: photon counts vs current comparison of different laser power of the $2.6 \cdot 10^{17}$ ion/cm^2 irradiated device.

into the possibility of enlarge the saturation region of operation of the detector through controllable helium ion irradiation.

Additionally, the same experiment has been repeated with a laser in the 1550 nm wavelength. Once again, due to the detector geometry and fabrication, none of our detectors where sensitive at this wavelengths. In the future, by testing a more starting sensitive device it would be very interesting try to investigate the possibility of extend the range of the spectral frequency sensitivity of the detectors simply exploiting the post-process helium ion irradiation, without changing their layout. Finally, we tried to investigate the different effect that parameters such as helium ion beam acceleration voltage could have on the superconductive film. All the previous devices has been irradiated with an ion beam with an acceleration voltage of 30 keV. A comparison with an acceleration voltage of 20 keV is shown in figure 4.21. As expected, for the detector metrics point of view no relevant difference can be observed. Further investigation on the properties of the material such as morphological, topological and optical properties.

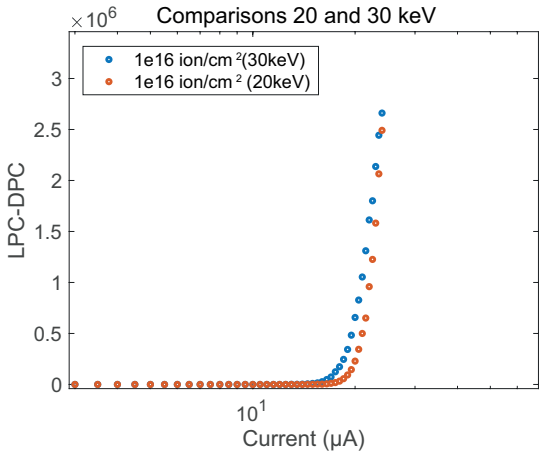

Figure 4.21: Comparison photon count vs current for SNSPDs irradiated with acceleration voltage of 20 keV and 30 keV and same dose (10^{16} ion/cm^2).

Chapter 5

Conclusion and perspectives

In conclusion, in this thesis we investigated the effects of helium ion radiation on NbN nanowires and NbN and MgB_2 superconducting nanowire single photon detectors (SNSPDs). The analytical and experimental findings presented in this thesis highlight the big potential of helium irradiation as a post-process for superconducting nanowires single-photon detectors.

Firstly, simulations were conducted to model the interaction of helium ions with NbN and MgB_2 target materials. The SRIM modeling tool was utilized to compare various parameters to control the irradiation process, providing valuable insights for future experimental investigations. Then, a testing device was designed and fabricated for irradiation experiments aimed at enhancing detector metrics at low doses and inducing superconductivity destruction at high doses. Unfortunately, for MgB_2 the enhancement of detector sensitivity could not be achieved due to sample destruction, highlighting the fragile nature of this material. Future studies could explore detectors with lower fill factors and silicon capping layers to address this challenge. For NbN single nanowires, the reduction of the switching current and destruction of superconductivity were successfully demonstrated with high doses. This resulted in the creation of a bias resistor, paving the way for utilizing helium ions to generate controlled resistances, potentially through the implementation of multiple cuts over the wire. Additionally, an enhancement in detection efficiency was achieved for NbN SNSPDs through helium irradiation at lower doses. However, saturation of the detectors was not attained, prompting further exploration with thinner detectors and lower fill factors to investigate the impact of irradiation in the saturation operation region, including parameters such as superconductive bandgap and reset time. Moreover, thinner superconducting layers offer the potential to observe finer variations in critical current and detector metrics, allowing for an investigation into the intrinsic factors contributing to these phenomena.

Additionally, parameters like detector time jitter and critical temperature should be analyzed in future studies. Moreover, considering the big potential of helium irradiation, efficient control of this phenomenon would be of great interest. Notably, the exposure time required to achieve the dose used in this experiment was long. To address this, future approaches could explore increasing or eliminating the numerical aperture in the helium gun or raising the beam current beyond 5 pA. Finally, this study has shown how helium irradiation affects NbN and MgB_2 materials, demonstrating its potential in improving detector performance and obtaining controlled resistances. The results establish the foundation for subsequent research which could involve further optimization of the irradiation process, exploration of alternative materials and device configurations, and deepening of our understanding of its underlying mechanisms.

Bibliography

[1] Iman Esmaeil Zadeh, J Chang, Johannes WN Los, Samuel Gyger, Ali W Elshaari, Stephan Steinhauer, Sander N Dorenbos, and Val Zwiller. Superconducting nanowire single-photon detectors: A perspective on evolution, state-of-the-art, future developments, and applications. *Applied Physics Letters*, 118(19):190502, 2021.

[2] Weijun Zhang, Qi Jia, Lixing You, Xin Ou, Hao Huang, Lu Zhang, Hao Li, Zhen Wang, and Xiaoming Xie. Saturating intrinsic detection efficiency of superconducting nanowire single-photon detectors via defect engineering. *Physical Review Applied*, 12(4):044040, 2019.

[3] AP Drozdov, MI Eremets, IA Troyan, Vadim Ksenofontov, and Sergii I Shylin. Conventional superconductivity at 203 kelvin at high pressures in the sulfur hydride system. *Nature*, 525(7567):73–76, 2015.

[4] Emma Lomonte, Martin A Wolff, Fabian Beutel, Simone Ferrari, Carsten Schuck, Wolfram HP Pernice, and Francesco Lenzini. Single-photon detection and cryogenic reconfigurability in lithium niobate nanophotonic circuits. *Nature communications*, 12(1):6847, 2021.

[5] Glenn D Martinez, Drew Buckley, Ilya Charaev, Andrew Dane, Douglas E Dow, and Karl K Berggren. Superconducting nanowire fabrication on niobium nitride using helium ion irradiation. *arXiv preprint arXiv:2003.02898*, 2020.

[6] Shane A Cybart, EY Cho, TJ Wong, Björn H Wehlin, Meng K Ma, Chuong Huynh, and RC Dynes. Nano josephson superconducting tunnel junctions in y-ba-cu-o direct-patterned with a focused helium ion beam. *arXiv preprint arXiv:1409.4876*, 2014.

[7] François Couëdo, Paul Amari, Cheryl Feuillet-Palma, Christian Ulysse, Yogesh Kumar Srivastava, Ranjan Singh, Nicolas Bergeal, and Jérôme Lesueur. Dynamic properties of high-t c superconducting nano-junctions made with a focused helium ion beam. *Scientific Reports*, 10(1):10256, 2020.

[8] Chen Zhang, Da Wang, Zheng-Hao Liu, Yan Zhang, Ping Ma, Qing-Rong Feng, Yue Wang, and Zi-Zhao Gan. Fabrication of superconducting nanowires from ultrathin mgb2 films via focused ion beam milling. *AIP Advances*, 5(2):027139, 2015.

[9] Ilya Charaev, DA Bandurin, AT Bollinger, IY Phinney, I Drozdov, M Colangelo, BA Butters, T Taniguchi, K Watanabe, X He, et al. Single-photon detection using high-temperature superconductors. *arXiv preprint arXiv:2208.05674*, 2022.

[10] WE Pickett. Electron-phonon coupling in mgb2-like materials: its magnitude and its limits. *Brazilian Journal of Physics*, 33:695–699, 2003.

[11] Rebecca J Nicholls, Sofia Diaz-Moreno, William Iliffe, Yatir Linden, Tayebeh Mousavi, Matteo Aramini, Mohsen Danaie, Chris RM Grovenor, and Susannah C Speller. Understanding irradiation damage in high-temperature superconductors for fusion reactors using high resolution x-ray absorption spectroscopy. *Communications Materials*, 3(1):52, 2022.

[12] Sergey Cherednichenko, Narendra Acharya, Evgenii Novoselov, and Vladimir Drakinskiy. Low kinetic inductance superconducting mgb2 nanowires with a 130 ps relaxation time for single-photon detection applications. *Superconductor Science and Technology*, 34(4):044001, 2021.

[13] Holger Bartolf. *Fluctuation Mechanisms in Superconductors*, pages 181–184. Springer Fachmedien Wiesbaden, Wiesbaden, 2016.

[14] Stefan Strohauer, Fabian Wietschorke, Lucio Zugliani, Rasmus Flaschmann, Christian Schmid, Stefanie Grotowski, Manuel Müller, Björn Jonas, Matthias Althammer, Rudolf Gross, et al. Site-selective enhancement of superconducting nanowire single-photon detectors via local helium ion irradiation. *arXiv preprint arXiv:2305.14175*, 2023.

[15] Michael Tinkham. *Introduction to superconductivity*. Courier Corporation, 2004.

[16] Ion implantation. `https://inst.eecs.berkeley.edu/~ee143/fa16/lectures/Lecture07-Ion%20Implantation.pdf`. Accessed on [Insert Access Date].

[17] James F Ziegler, Matthias D Ziegler, and Jochen P Biersack. Srim–the stopping and range of ions in matter (2010). *Nuclear Instruments and Methods in Physics Research Section B: Beam Interactions with Materials and Atoms*, 268(11-12):1818–1823, 2010.

[18] Stanley Wolf and Richard N Tauber. Silicon processing for the vlsi era, vol. 1, lattice press. *Sunset Beach, CA*, page 441, 1986.

[19] Sujoy Ghosh. *Effect of Microstructure and Rare Earth Doping on Superconducting Properties of MgB 2 Bulk Processed by Spark Plasma Sintering*. University of California, Davis, 2021.

[20] Suhan Yin, Jia Liu, Yiyuan Kang, Yuqing Lin, Dongjian Li, and Longquan Shao. Interactions of nanomaterials with ion channels and related mechanisms. *British Journal of Pharmacology*, 176(19):3754–3774, 2019.

[21] Carl Zeiss Microscopy GmbH. Carl Zeiss Microscopy GmbH. `https://www.zeiss.com/microscopy/home.html`. Accessed on [Insert Access Date].

[22] WJ Skocpol, MR Beasley, and M Tinkham. Self-heating hotspots in superconducting thin-film microbridges. *Journal of Applied Physics*, 45(9):4054–4066, 1974.

[23] Michihide Kitamura, Kazuhiro Yamaki, and Akinobu Irie. Nonequilibrium effect in ferromagnet-insulator-superconductor tunneling junction currents. *World Journal of Condensed Matter Physics*, 6(3), July 2016.

[24] A. Annunziata. Single-photon detection, kinetic inductance, and non-equilibrium dynamics in niobium and niobium nitride superconducting nanowires. 2010.

[25] Chandra M Natarajan, Michael G Tanner, and Robert H Hadfield. Superconducting nanowire single-photon detectors: physics and applications. *Superconductor science and technology*, 25(6):063001, 2012.